

Expanded Organic Building Units for the Construction of Highly Porous Metal–Organic Frameworks

Guo-Qiang Kong,^[a] Zhi-Da Han,^[a] Yabing He,^[b] Sha Ou,^[a] Wei Zhou,^[c, d]
Taner Yildirim,^[d, e] Rajamani Krishna,*^[f] Chao Zou,^[a] Banglin Chen,*^[b] and
Chuan-De Wu*^[a]

Abstract: Two new organic building units that contain dicarboxylate sites for their self-assembly with paddle-wheel $[\text{Cu}_2(\text{CO}_2)_4]$ units have been successfully developed to construct two isorecticular porous metal–organic frameworks (MOFs), ZJU-35 and ZJU-36, which have the same topology (Reticular Chemistry Structure Resource (RCSR) symbol) as HKUST-1. Because the organic linkers in ZJU-35 and ZJU-36 are systematically enlarged, the pores in these two new porous MOFs vary from 10.8 Å in HKUST-1 to 14.4 Å in ZJU-35 and 16.5 Å in ZJU-36, thus leading to their higher porosities with Brunauer–Emmett–Teller (BET) surface areas of 2899 and 4014 $\text{m}^2 \text{g}^{-1}$ for ZJU-35 and ZJU-36, respectively. High-pressure gas-sorption isotherms indicate that both ZJU-35 and ZJU-36 can take up large amounts of CH_4 and CO_2 , and

are among the few porous MOFs with the highest volumetric storage of CH_4 under 60 bar and CO_2 under 30 bar at room temperature. Their potential for high-pressure swing adsorption (PSA) hydrogen purification was also preliminarily examined and compared with several reported MOFs, thus indicating the potential of ZJU-35 and ZJU-36 for this important application. Studies show that most of the highly porous MOFs that can volumetrically take up the greatest amount of CH_4 under 60 bar and CO_2 under 30 bar at room temperature are those self-assembled from organic tetra- and hexacarboxylates that contain *m*-benzenedicarboxylate units with the $[\text{Cu}_2(\text{CO}_2)_4]$ units,

because this series of MOFs can have balanced porosities, suitable pores, and framework densities to optimize their volumetric gas storage. The realization of the two new organic building units for their construction of highly porous MOFs through their self-assembly with $[\text{Cu}_2(\text{CO}_2)_4]$ units has provided great promise for the exploration of a large number of new tetra- and hexacarboxylate organic linkers based on these new organic building units in which different aromatic backbones can be readily incorporated into the frameworks to tune their porosities, pore structures, and framework densities, thus targeting some even better performing MOFs for very high gas storage and efficient gas separation under high pressure and at room temperature in the near future.

Keywords: adsorption • gas storage • metal–organic frameworks • self-assembly • surface analysis

Introduction

The last two decades have witnessed the emergence of and significant progress in porous metal–organic frameworks (MOFs) and/or porous coordination polymers (PCPs).^[1,2] The concept for constructing such new porous materials is

quite straightforward: it makes use of metal–organic coordination bonds to assemble framework solids, the crystalline structures of which can survive under vacuum and/or thermal activation to generate pore spaces for the recognition of substrates, energy storage, and chemical transformations. Given the fact that some very simple Werner complexes

[a] Dr. G.-Q. Kong, Z.-D. Han, S. Ou, Dr. C. Zou, Prof. Dr. C.-D. Wu
Center for Chemistry of High-Performance and Novel Materials
Department of Chemistry, Zhejiang University
Hangzhou, 310027 (P.R. China)
Fax: (+86) 571-87951895
E-mail: cdwu@zju.edu.cn


[b] Dr. Y. He, Prof. Dr. B. Chen
Department of Chemistry, University of Texas at San Antonio
One UTSA Circle, San Antonio, Texas 78249-0698 (USA)
Fax: (+1) 210-458-7428
E-mail: banglin.chen@utsa.edu

[c] Dr. W. Zhou
Department of Materials Science and Engineering
University of Maryland, College Park, MD 20742 (USA)

[d] Dr. W. Zhou, Prof. Dr. T. Yildirim
NIST Center for Neutron Research
Gaithersburg, MD 20899-6102 (USA)

[e] Prof. Dr. T. Yildirim
Department of Materials Science and Engineering
University of Pennsylvania, Philadelphia, PA 19104-6272 (USA)

[f] Prof. Dr. R. Krishna
Van 't Hoff Institute of Molecular Science
University of Amsterdam, Science Park 904
1098 XH Amsterdam (The Netherlands)
E-mail: r.krishna@uva.nl

 Supporting information for this article is available on the WWW under <http://dx.doi.org/10.1002/chem.201302515>.

such as $[\text{Ni}(\text{4-Me-pyridine})_4(\text{NCS})_2]$ can take up gas molecules,^[3] coordination polymers might be able to exhibit gas/vapor sorption as well, as proposed by Hoskins and Robson in 1989.^[4] However, it took quite long time to realize the first several porous coordination polymers and to introduce the term metal-organic frameworks, the permanent porosities of which were established by gas-sorption isotherms during 1997 to 1999.^[5] This is mainly because most so-called crystallographically “porous” coordination polymers are not robust enough to sustain the vacuum/thermal activation: once the solvent guest molecules are removed from the pore spaces of the coordination polymers, the frameworks collapse.^[6] Such phenomena once again confirmed Aristotle’s famous statement “Nature abhors the vacuum”.

The establishment of the permanent porosities of the first several prototypic MOFs has immediately initiated much more extensive research endeavors on functional MOF materials for gas storage, separation, heterogeneous catalysis, photonics, and drug delivery.^[7–11] From the structure point of view, porous MOFs are self-assembled from metal ions and/or metal-containing clusters (so-called metal-containing secondary building units (SBUs)) and organic building units and/or linkers.^[12] Such a MOF structure rationalization can help us to readily understand the structures and pore dimensions of MOF materials, and nowadays is widely practiced in the rational synthesis of MOFs. This is particularly true for those MOFs constructed from $[\text{Zn}_4\text{O}(\text{CO}_2)_6]$ and $[\text{Cu}_2(\text{CO}_2)_4]$ SBUs and organic carboxylates.

$[\text{Zn}_4\text{O}(\text{CO}_2)_6]$ and $[\text{Cu}_2(\text{CO}_2)_4]$ SBUs are two of the most useful inorganic building units for the construction of highly porous MOFs with BET surface areas over $2000 \text{ m}^2 \text{ g}^{-1}$. Since the discovery of MOF-5 (or IRMOF-1),^[5c] the $[\text{Zn}_4\text{O}(\text{CO}_2)_6]$ units have not only been assembled with a number of bicarboxylates to synthesize a series of isorecticular MOFs whose pore spaces can be systematically varied by the length of the bicarboxylates,^[13] but have been also connected with tricarboxylates such as 1,3,5-tris(4-carboxyphenyl)benzene (BTB) to generate another highly porous MOF-177.^[14] Matzger and Kaskel have even been able to assemble two different types of organic carboxylates such as benzene-1,4-dicarboxylate (BDC) and BTB with $[\text{Zn}_4\text{O}(\text{CO}_2)_6]$ units leading to a number of exceptionally highly porous MOFs.^[15] For example, MOF-200 and -205 developed by Yaghi have BET surface areas of 4530 and $6240 \text{ m}^2 \text{ g}^{-1}$, respectively.^[16]

$[\text{Cu}_2(\text{CO}_2)_4]$ SBUs have been even more widely utilized than $[\text{Zn}_4\text{O}(\text{CO}_2)_6]$ ones to generate highly porous MOFs. The $[\text{Cu}_2(\text{CO}_2)_4]$ unit can be topologically considered as a square-planar node. Self-assembly of $[\text{Cu}_2(\text{CO}_2)_4]$ units with linear bicarboxylates led to the formation of two-dimensional (4,4) square-planar nets.^[17] When the bicarboxylate is twisted, as in the case of 2-bromobenzene-1,4-dicarboxylate, a three-dimensional NbO type of porous MOF-101 can be constructed.^[18] It is understandable that self-assembly of $[\text{Cu}_2(\text{CO}_2)_4]$ units with organic carboxylates of three dimensions can lead to three-dimensional porous MOFs, as exemplified in MOF-11,^[19] MOF-14,^[20] PCN-6,^[21]

and many others.^[22] During the extensive studies on the $[\text{Cu}_2(\text{CO}_2)_4]$ -based porous MOFs, the community realized that some organic carboxylates such as BTB have a limited capacity to assemble with $[\text{Cu}_2(\text{CO}_2)_4]$ to construct highly porous MOFs because of the framework interpenetration and/or the unstable frameworks. In fact, although the BTB organic linker is quite large, the resulting MOF-14 is only moderately porous with a BET surface area of $1502 \text{ m}^2 \text{ g}^{-1}$ because of the framework interpenetration, whereas the non-interpenetrated MOF-14 (MOF-143) from BTB and the doubly interpenetrated MOF-388 from an even larger tricarboxylate (TAPB) are nonporous.^[23] Studies, however, also show that some organic carboxylates, particularly those containing *m*-benzenedicarboxylate, are favorable to the formation of stable porous MOFs. The well-known porous MOF constructed from $[\text{Cu}_2(\text{CO}_2)_4]$ units and *m*-benzenedicarboxylate containing carboxylates is HKUST-1 ($\text{Cu}_3(\text{BTC})_2$; BTC = benzene-1,3,5-tricarboxylate).^[5d] The incorporation of expanded organic linkers containing *m*-benzenedicarboxylate units into $[\text{Cu}_2(\text{CO}_2)_4]$ units, to a certain extent, was initiated by Chen et al. and subsequently by Lin et al. on *m*-benzenedicarboxylate containing tetracarboxylates.^[24] These works immediately attracted wide attention in the MOF community: not only a large number of tetracarboxylates, but also a number of hexacarboxylates containing *m*-benzenedicarboxylate have been readily assembled with $[\text{Cu}_2(\text{CO}_2)_4]$ units to generate highly porous MOFs.^[22] Although the mechanism as to why such *m*-benzenedicarboxylates containing carboxylates can stabilize the frameworks is not exclusively clear at this moment, the power of these *m*-benzenedicarboxylate units to stabilize the cages of moderate sizes surrounded by *m*-benzenedicarboxylate- $[\text{Cu}_2(\text{CO}_2)_4]$ framework surfaces certainly plays a very important role. The *meta* position of the two carboxylates within the organic linkers can also minimize the possibility of the framework interpenetration. The implementation of supercritical carbon dioxide activation has now led to two extremely porous MOFs with BET surface areas over $7000 \text{ m}^2 \text{ g}^{-1}$, which have been generated from two hexacarboxylate organic linkers built from three *m*-benzenedicarboxylate units.^[25]

Motivated by the power of this basic *m*-benzenedicarboxylate organic building unit to construct highly porous MOFs, we have been working on the expanded organic units, as shown in Figure 1a (**II** and **III**), for the design of new organic linkers and thus porous MOFs through their self-assembly with the paddle-wheel $[\text{Cu}_2(\text{CO}_2)_4]$ SBUs. To the best of our knowledge, such expanded organic units have never been utilized before. If such organic building units, particularly unit **III** as shown in Figure 1a, can assemble with $[\text{Cu}_2(\text{CO}_2)_4]$ units to construct porous MOFs, the incorporation of this new organic unit into the rich organic aromatic backbones will lead to an abundance of new organic linkers for the construction of highly porous MOFs (Figure S2 in the Supporting Information). Theoretically speaking, all the aromatic backbones utilized for the syntheses of tetra- and hexacarboxylic acids containing *m*-benzenedicarboxylate organ-

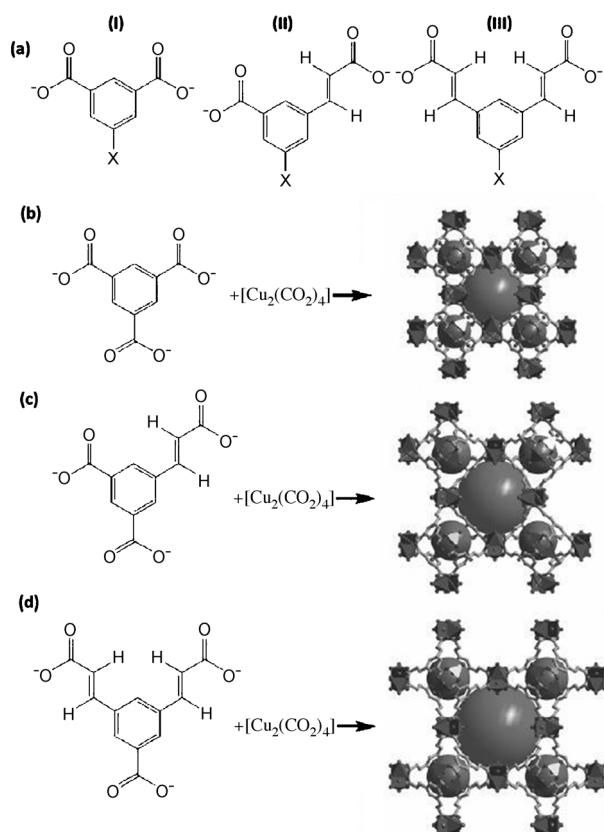


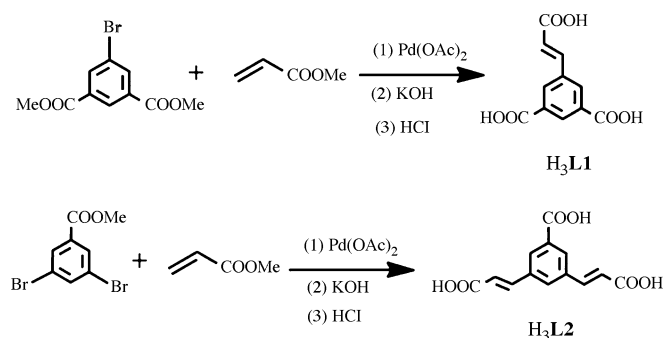
Figure 1. a) *m*-Benzenedicarboxylate organic building unit **I** and two new expanded ones (**II** and **III**). Self-assembly of b) H_3 BTC and c,d) two new organic linkers with paddle-wheel $[Cu_2(CO_2)_4]$ units leading to the construction of isoreticular porous MOFs: b) HKUST-1, c) ZJU-35, and d) ZJU-36, the pores of which (small and large spheres) are systematically enlarged (Cu, polyhedral, H atoms are omitted for clarity).

ic building unit **I** (Figure 1) can be also explored for the syntheses of new organic linkers of tetra- and hexacarboxylic acids containing organic building unit **III** (Figure 1) and thus for the construction of highly porous MOFs. Herein we report the first two examples of organic linkers (Figure 1c,d) constructed from such new expanded organic building units and correspondingly constructed highly porous MOFs (ZJU-35 and ZJU-36; ZJU = Zhejiang University) self-assembled from these two new tricarboxylates and $[Cu_2(CO_2)_4]$ units. Because these two new organic linkers can be considered as the expanded organic linkers of BTC, the resulting porous MOFs ZJU-35 and ZJU-36 are isoreticular to HKUST-1 and thus have the same tbo topology (Reticular Chemistry Structure Resource (RCSR) symbol) (Figure 1b).^[12c] Of course, ZJU-35 and ZJU-36 exhibit higher porosities than HKUST-1 because of their enlarged pore spaces, with BET surface areas of 2899 and 4014 $m^2 g^{-1}$, respectively. Their potential applications for high-pressure gas storage (H_2 , CH_4 , and CO_2) and CO_2/H_2 separation were examined, showing high storage and separation capacities for these gas molecules. The bright promise of the organic building unit **III** for the construction of new expanded or-

ganic linkers and thus highly porous MOFs will lead to a number of highly porous MOFs for gas storage and separation in the near future.

Results and Discussion

As shown in Scheme 1, the two new tricarboxylate organic linkers 5-(2-carboxyvinyl)isophthalic acid (H_3 L1) and 3,3'-(5-carboxy-1,3-phenylene)diacrylic acid (H_3 L2) were simply



Scheme 1. The synthetic schemes for the organic linkers H_3 L1 and H_3 L2.

synthesized by Heck cross-coupling reactions of methylated bromophenylcarboxylate and methyl acrylate, followed by hydrolysis and acidification. Reactions of these two organic linkers with $Cu(NO_3)_2 \cdot 3H_2O$ in acidified DMF/ H_2O at 65 °C for two days afforded blue crystals of ZJU-35 and ZJU-36, respectively. The compositions of the as-synthesized MOFs were based on the elemental analyses, thermogravimetric analyses (TGA), and single-crystal structures.

Single-crystal X-ray diffraction analysis revealed that the two MOFs are isomorphous, and crystallize in the cubic $Fm\bar{3}m$ space group. Both ZJU-35 and ZJU-36 are isoreticular with the very important prototype MOF HKUST-1 of the tbo topology, although the new linkers H_3 L1 and H_3 L2 are apparently less symmetric than H_3 BTC. It has been rationalized that the self-assembly of tricarboxylate with paddle-wheel $[Cu_2(CO_2)_4]$ either forms tbo or pto frameworks, which are attributed to the different structural orientation of tritopic carboxylates.^[20,21,23,26] Because H_3 L1 and H_3 L2 are larger than H_3 BTC, the pores within these isoreticular MOFs are systematically enlarged: the small orange pockets are 5.3, 6.4, and 7.5 Å, and the large purple cages are 10.8, 14.4, and 16.5 Å in HKUST-1, ZJU-35, and ZJU-36, respectively, taking into account the van der Waals radius, as shown in Figure 1. PLATON calculations indicate that the void spaces are 62.3 and 76.9% for ZJU-35 and ZJU-36, respectively.^[27]

Both activated ZJU-35a and ZJU-36a exhibit type I reversible sorption isotherms and take up 747 and 1033 $cm^3 g^{-1}$ N_2 at 77 K and 1 bar, respectively (Figure 2a). Accordingly, ZJU-35a has a BET surface area of 2899 $m^2 g^{-1}$ and a pore volume of 1.156 $cm^3 g^{-1}$, whereas ZJU-36a has a BET surface area of 4014 $m^2 g^{-1}$ and a pore volume of 1.599 $cm^3 g^{-1}$.

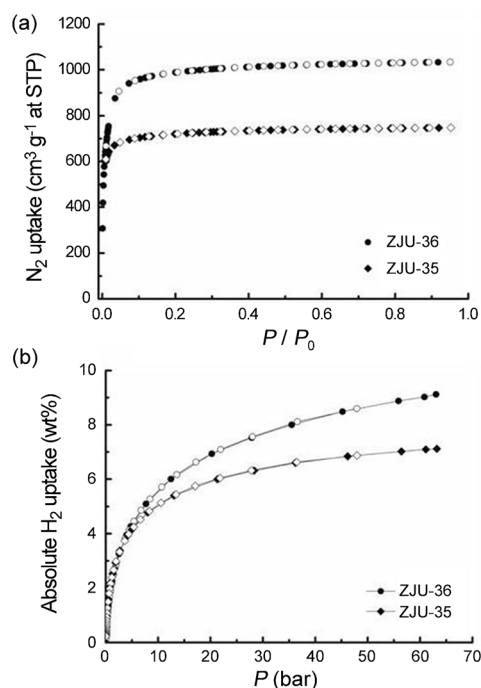


Figure 2. a) N₂ and b) absolute H₂ sorption isotherms of ZJU-35a and ZJU-36a at 77 K. STP = standard temperature and pressure.

The porosities of both ZJU-35a and ZJU-36a are systematically higher than those of HKUST-1 with a BET surface area of 1502 m² g⁻¹ and a pore volume of 0.76 cm³ g⁻¹, and are among the few highly porous MOFs. The maximum excess H₂ uptake of ZJU-35a and ZJU-36a is 5.2 and 6.2 wt% (Figure S9 in the Supporting Information), respectively, which correlates well with their corresponding surface areas. Their absolute H₂-storage capacities are 7.1 and 9.1 wt%, respectively, at 77 K and 63 bar (Figure 2b), which is moderately high. Their room-temperature absolute hydrogen-storage values are 1.0 and 1.2 wt% for ZJU-35a and ZJU-36a, respectively.

The CH₄-storage capacities of ZJU-35a and ZJU-36a are 227 and 203 cm³ cm⁻³, respectively, at 300 K and 64 bar (Figure 3a). ZJU-35a and ZJU-36a have high CO₂ uptakes of 328 and 311 cm³ cm⁻³, respectively, at 300 K and 30 bar. ZJU-35a and ZJU-36a are among the few best-performing MOF materials for the storage and capture of

CH₄ and CO₂ volumetrically at room temperature. The comparison of some highly porous MOFs for CH₄ and CO₂ storage and capture is summarized in Tables S2 and S3 in the Supporting Information. Because little data are available for CH₄ storage above 60 bar, and for CO₂ capture above 30 bar, we compare the CH₄ and CO₂ storage capacities of our MOFs under 60 and 30 bar, respectively, at room temperature.

As shown in Figure 3b, the gravimetric CH₄-storage capacities of the MOF materials under 60 bar and at room temperature are basically dependent on their BET surface areas. The larger the surface area, the larger the absolute CH₄ uptake by the MOF. Accordingly, MOF-210 and DUT-49 have the maximum gravimetric methane uptakes of 536 and 540 cm³ g⁻¹, respectively, at RT and 60 bar because of their extremely high BET surface areas of 6240 and 5476 m² g⁻¹, among those examined porous MOFs for methane storage.^[16,28] Because the framework density is inversely proportional to the pore volume of the MOF materials, as shown in Figure 3d (1/(framework density) is basically linearly correlated to the pore volume of the framework)—the larger the porosity, the smaller the framework density of the MOF—those MOFs exhibiting high volumetric methane storage should have balanced porosities and framework densities to utilize the pore spaces efficiently. In fact, these MOFs have absolute volumetric CH₄ uptakes of over 220 cm³ cm⁻³ under 60 bar at room temperature and have BET surfaces from 1218 m² g⁻¹ for NiMOF-74 to 3342 m² g⁻¹ for NOTT-102.^[29,30] Of course, the M-MOF-74 series of

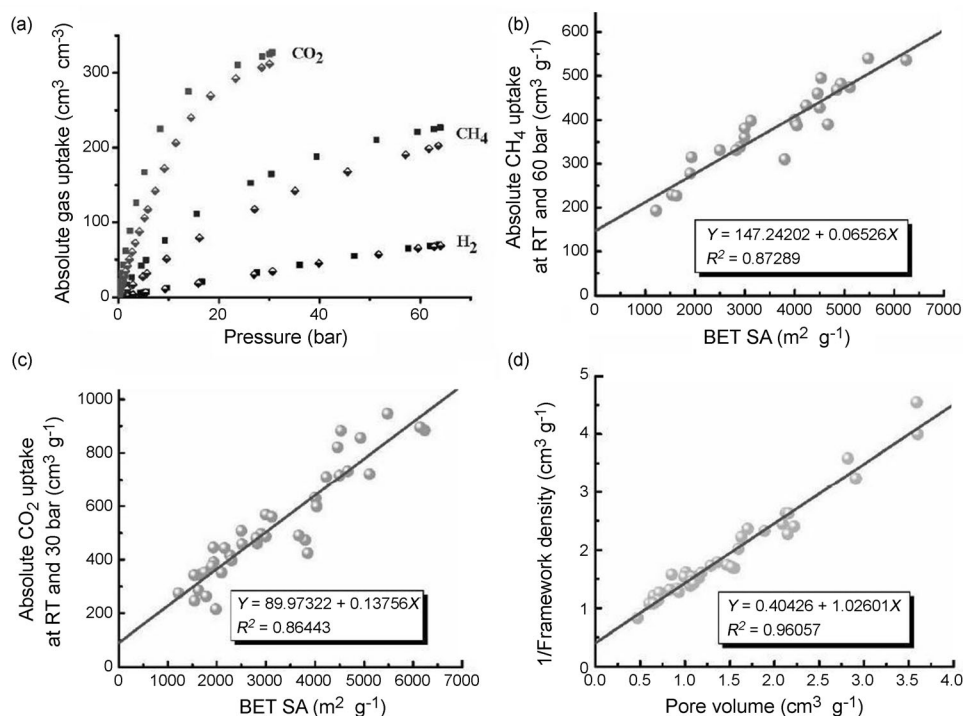


Figure 3. a) Absolute gas-sorption isotherms of CO₂, CH₄, and H₂ of ZJU-35a (■) and ZJU-36a (open-solid diamond) at 300 K; the relationship between the gravimetric b) CH₄ and c) CO₂ storage capacities of the MOF materials with BET surface areas, and d) the plot of the 1/framework density versus the framework pore volume. SA = surface area.

MOFs are very special because of their significantly high densities of open metal sites for the CH₄ storage. In terms of deliverable methane capacities (60 to 5 bar), NU-125 and NOTT-102 have the highest volumetric deliverable amounts of methane of 183 and 182 cm³cm⁻³, respectively.^[30,31] ZJU-35 is among the six MOFs whose volumetric deliverable amounts of methane are over 175 cm³cm⁻³. It needs to be mentioned that those MOFs with high densities of open metal sites such as the M-MOF-74 series exhibit quite low volumetric deliverable amounts of methane. This is because even at a pressure of 5 bar, this type of MOF can take up quite a large amount of methane, which limits their deliverable amount of methane capacity.

The absolute gravimetric CO₂ capture capacities of the MOF materials under 30 bar and at room temperature are also approximately linearly dependent on their BET surface areas, as shown in Figure 3c. DUT-49 has the highest absolute gravimetric CO₂ uptake of 947 cm³g⁻¹ at RT and 30 bar.^[28] To reach high volumetric CO₂ uptake at RT and 30 bar, the MOF materials also need to have balanced porosities and framework densities to maximize the pore-usage efficiency. Until now, NU-111 had the highest absolute volumetric CO₂ uptake of 350 cm³cm⁻³ at RT and 30 bar.^[32] ZJU-35 is one of the six MOFs with absolute volumetric CO₂ uptake amounts of over 320 cm³cm⁻³ at RT and 30 bar. The BET values of these six MOFs are in the range of 1931 m²g⁻¹ in PCN-11 to 4930 m²g⁻¹ in NU-111 except the significantly low one of 1218 m²g⁻¹ in Ni-MOF-74.^[29,32,33] Again, the significantly high volumetric CO₂ uptake of Ni-MOF-74 is attributed to the high density of open Ni²⁺ sites within this porous MOF.

Close examination of these data also indicates that those MOFs exhibiting high absolute volumetric CH₄ storage under 60 bar and high deliverable amounts of methane (60 to 5 bar), and high absolute volumetric CO₂ capture under 30 bar and at room temperature are mainly those MOFs constructed from [Cu₂(CO₂)₄] units with tetra- or hexacarboxylates containing *m*-benzenedicarboxylate units (building unit **I** in Figure 1a) except M-MOF-74, MOF-205, MIL-101c, and our reported ZJU-35 and -36.^[16,29,34] Because building unit **III** can be simply considered as the expanded building unit **I**, this new organic building unit is expected to produce a number of tetra- and hexacarboxylic acids with different aromatic backbones as the organic linkers, and thus to self-assemble with [Cu₂(CO₂)₄] units to construct a series of highly porous MOFs for their high CH₄ storage and CO₂ capture at room temperature.

The high CH₄ storage and CO₂ capture of these two new MOFs at room temperature also encouraged us to examine their potential applications on hydrogen purification, which is one very important industrial process for which optimized adsorbents are urgently needed because small improvements can result in significant energy savings and cost reductions.^[36–38] To establish the feasibility of ZJU-35a and ZJU-36a for high-pressure swing adsorption (PSA) purification of hydrogen, we studied in detail their isosteric heats of adsorption, Q_{st} , of CO₂, adsorption selectivity, and packed-bed

adsorber breakthrough simulation for a ternary 30:20:50 CO₂/CH₄/H₂ gas mixture (Figure S20 in the Supporting Information), which is typically encountered in H₂-purification processes. Because very few porous MOFs have been comprehensively examined for their temperature- and pressure-dependent sorption isotherms for all H₂, CH₄, and CO₂ gas molecules, we compared the performances of ZJU-35a and ZJU-36a with other MOFs (HKUST-1, MgMOF-74, Cu-TDPAT, and MIL-101) and zeolites (NaX and LTA-5A).^[36–38]

As shown in Figure 4a, the Q_{st} values of CO₂ systematically decrease from HKUST-1 to ZJU-35a and then to ZJU-36a because the pores are enlarged while the densities of the open metal sites are reduced gradually within these isorecticular MOFs. Cu-TDPAT has very high Q_{st} values of CO₂, particularly at low loading of CO₂, because of its amine groups on the pore surfaces for their very strong interactions with CO₂. The very large Q_{st} values of CO₂ for MgMOF-74 are attributed to the strong electrostatic interactions between open Mg²⁺ sites and CO₂ molecules. Zeolites NaX and LTA-5A with smaller pores have larger Q_{st} values of CO₂ than ZJU-35a and ZJU-36a.

HKUST-1 has the highest, and ZJU-36a has the lowest CO₂/H₂ and CH₄/H₂ IAST adsorption selectivity among the three isorecticular porous MOFs (Figures S21 and S22 in the Supporting Information).^[35] The performance of a PSA unit is dictated both by the adsorption selectivity and by the capacity to adsorb both CO₂ and CH₄. Generally speaking, higher capacities are desirable because the adsorber bed can be run for longer lengths of time before the need for regeneration arises. The sum of the component loadings of CO₂ and CH₄ in the mixture is an appropriate measure of the capacity. Figure 4b presents data on the IAST calculations of the (CO₂+CH₄) uptake capacities, which indicate that ZJU-35a and ZJU-36a have higher uptake capacities than other examined materials for pressures exceeding 2 MPa.

Transient breakthrough calculations demonstrate that hydrogen breaks through earliest and it is possible to produce pure hydrogen from this three-component mixture during the adsorption cycles of both ZJU-35a and ZJU-36a (Figure 4c and Figure S23 in the Supporting Information).^[39] The most important feature is that ZJU-35a exhibits significantly high gravimetric hydrogen productivity, as shown in Figure 4d. For pressures exceeding 4 MPa, typical of hydrogen purification, the hierarchy of productivities is ZJU-35a > MgMOF-74 ≈ Cu-TDPAT ≈ HKUST-1 ≈ ZJU-36a > NaX > MIL-101 > LTA-5A. The excellent performance of ZJU-35a is due to the suitable combination of separation selectivities and capacities optimized for H₂ purification.

The relative costs of regeneration of the bed will be largely dictated by the desorption of the CO₂ captured during the interval 0– τ_{break} . As shown in Figure 4a, the energy required for regeneration of adsorbed CO₂ in fixed-bed adsorbents will be lower for ZJU-35a and ZJU-36a than for HUKST-1, MgMOF-74, and Cu-TDPAT. For pressures exceeding 4 MPa (Figure 4d), ZJU-35a and ZJU-36a have higher gravimetric production capacities than other examined

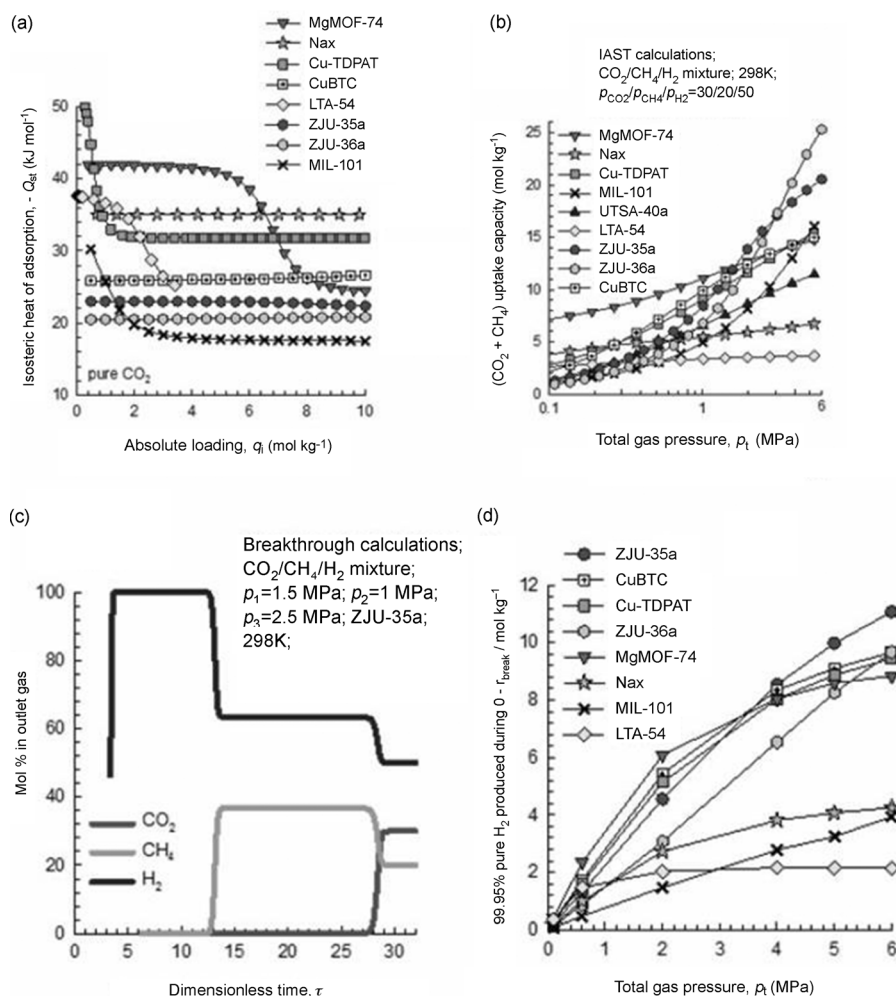


Figure 4. a) Comparison of isosteric heats of adsorption, Q_{st} , of CO₂ in ZJU-35a, ZJU-36a, CuBTC (HKUST-1), MgMOF-74, Cu-TDPAT, MIL-101, NaX, and LTA-5A. The calculations of Q_{st} are based on the use of the Clausius–Clapeyron equation. b) Calculations using ideal adsorbed solution theory (IAST) of Myers and Prausnitz^[35] (CO₂ + CH₄) uptake capacity, expressed as moles per kg of adsorbent, in equilibrium with a ternary CO₂/CH₄/H₂ 30:20:50 gas mixture maintained under isothermal conditions at 298 K. c) Breakthrough characteristics of an adsorber packed with ZJU-35a maintained at isothermal conditions at 298 K and 5 MPa. d) Influence of the operating pressure on the number of moles of 99.95% + pure H₂ produced per kg of adsorbent material during the time interval 0– τ_{break} . The breakthrough times, τ_{break} , correspond to those when the outlet gas contains 500 ppm (CO₂ + CH₄).

MOFs. Among the three isoreticular MOFs, ZJU-35a has the highest gravimetric hydrogen production capacity whereas HKUST-1 has the highest volumetric hydrogen production capacity (Figure S25 in the Supporting Information) at high pressures. Overall, ZJU-35a can be ranked as one of the few best porous MOFs for high-pressure hydrogen purification when regeneration cost, gravimetric and volumetric production capacities need to be balanced. The pore and channel sizes/curvatures, pore surface functionalities, pore volumes, and framework densities should be equally considered and optimized to further realize better MOF materials for high-pressure hydrogen purification in the near future.

With systematically enlarged pore sizes and porosities, ZJU-35 and ZJU-36 are expected to be fully explored for other diverse functions as well. In fact, their isoreticular HKUST-1 is one of the most important prototype MOFs for their applications in gas storage, separation, heterogeneous catalysis, drug delivery, as host materials for the encapsulation of active catalysts and nanoparticles, and fabrication of film devices.^[40] The realization of ZJU-35 as a significant potential material for high-pressure swing adsorption hydrogen purification at room temperature indicates that it is practically feasible to realize high-performance materials for such important industrial applications through the deliberate control of the pore space and metrics of the porous MOFs.

Conclusion

In summary, we have successfully developed two new organic carboxylate building units and realized two tricarboxylate linkers for the construction of isoreticular porous MOFs ZJU-35 and ZJU-36 for their high CH₄ storage, CO₂ capture, and hydrogen purification under high pressure and room temperature, which have been compared with the reported MOFs comprehensively. Because a series of new organic linkers can be readily synthesized from such simple organic building units through the incorporation of different aromatic backbones, this work will stimulate extensive research on the construction of a variety of new highly porous MOFs in which their framework topologies and porosities can be readily tuned for their high-pressure gas storage and separation. The fact that the MOFs exhibiting very high volumetric storage and capture of both CH₄ and CO₂ are mainly those self-assembled from organic linkers containing *m*-benzenedicarboxylate units with paddle-wheel [Cu₂(CO₂)₄] SBUs, the new organic building units reported here will be very promising to target some novel highly porous MOFs with even higher storage capacities for CH₄ and CO₂ under high pressure and room temperature.

Experimental Section

Materials and methods: All of the chemicals were obtained from commercial sources and were used without further purification. IR spectra were collected from KBr pellets on a FTS-40 spectrophotometer. TGA was carried out under an N₂ atmosphere on a SDT Q600 instrument at a heating rate of 10 °C min⁻¹. Elemental analyses were performed on a ThermoFinnigan Flash EA 1112 Element Analyzer. Powder X-ray diffraction (PXRD) data were recorded on a RIGAKU D/MAX 2550/PC for CuK_α radiation (λ = 1.5406 Å). ¹H and ¹³C NMR spectra were recorded on a 500 MHz spectrometer in CDCl₃ or [D₆]DMSO and the chemical shifts were reported relative to an internal standard of TMS (0 ppm). A Micromeritics ASAP 2020 surface-area analyzer was used to measure gas-adsorption isotherms.

Synthesis of dimethyl 5-(3-methoxy-3-oxoprop-1-enyl)isophthalate (Me₃L1): As shown in Scheme 1, dimethyl 5-bromo-1,3-benzenedicarboxylate (13.65 g, 50 mmol), methyl acrylate (9 mL, 100 mmol), K₂CO₃ (10.35 g, 75 mmol), tetrabutyl ammonium bromide (TBAB) (3.22 g, 10 mmol), Pd(OAc)₂ (1.122 g, 5 mmol), and DMF (100 mL) were mixed in a 250 mL round-bottomed flask. The mixture was heated at 130 °C under stirring for 24 h. After the reaction was cooled down to room temperature, the mixture was poured into water and extracted with ethyl acetate three times. The combined organic phase was dried over anhydrous MgSO₄ and concentrated under vacuum. The residue was subjected to chromatography on silica gel (petroleum ether/CH₂Cl₂ 5:1). The solvent was removed under reduced pressure to give a white powder. Yield: 8.3 g (60%); ¹H NMR (500 MHz, CDCl₃): δ = 3.83 (s, 3H), 3.97 (s, 6H), 6.58 (d, J = 16.0 Hz, 1H), 7.73 (d, J = 16.0 Hz, 1H), 8.36 (s, 2H), 8.67 ppm (s, 1H); ¹³C NMR (125 MHz, CDCl₃): δ = 51.9, 52.6, 120.4, 131.4, 131.8, 132.8, 135.3, 142.5, 165.8, 166.8 ppm; IR (KBr pellet): ν̄ = 1733 (s), 1644 (m), 1560 (w), 1448 (m), 1436 (m), 1342 (m), 1253 (s), 1207 (m), 1176 (s), 1130 (w), 994 (m), 860 (w), 755 (m), 596 cm⁻¹ (w).

Synthesis of 5-(2-carboxyvinyl)isophthalic acid (H₃L1): Me₃L1 (3.9 g, 14 mmol) and KOH (210 mmol, 11.7 g) in THF (50 mL) and H₂O (50 mL) were heated at 60 °C for 12 h. After the mixture was cooled down to room temperature, THF was evaporated under reduced pressure. The pH value of the mixture was adjusted to 1 by using concentrated HCl. The precipitate was collected by filtration, washed with water several times, and dried at 50 °C to afford a white powder. Yield: 3.2 g (97%); ¹H NMR (500 MHz, [D₆]DMSO): δ = 6.64 (d, J = 16.0 Hz, 1H), 7.71 (d, J = 16.0 Hz, 1H), 8.37 (s, 2H), 8.49 ppm (s, 1H); ¹³C NMR (125 MHz, [D₆]DMSO): δ = 121.5, 131.0, 131.9, 133.1, 135.0, 142.0, 166.6, 167.3 ppm; IR (KBr pellet): ν̄ = 1701 (s), 1641 (m), 1603 (w), 1420 (m), 1274 (s), 1220 (s), 1103 (w), 982 (m), 903 (m), 871 (w), 763 (s), 695 (m), 603 (m), 519 cm⁻¹ (m).

Synthesis of dimethyl 3,3'-(5-(methoxycarbonyl)-1,3-phenylene)diacrylate (Me₃L2): As shown in Scheme 1, methyl 3,5-dibromobenzoate (14.7 g, 50 mmol), methyl acrylate (9 mL, 100 mmol), K₂CO₃ (10.35 g, 75 mmol), tetrabutyl ammonium bromide (TBAB) (3.22 g, 10 mmol), Pd(OAc)₂ (1.122 g, 5 mmol), and DMF (100 mL) were mixed in a 250 mL round-bottomed flask. The mixture was heated at 130 °C under stirring for 24 h. After the reaction was cooled down to room temperature, the mixture was poured into water and extracted with ethyl acetate three times. The combined organic phase was dried over anhydrous MgSO₄ and concentrated under vacuum. The residue was subjected to chromatography on silica gel (petroleum ether/CH₂Cl₂ 5:1). The solvent was removed under reduced pressure to give a white powder. Yield: 9.9 g (65%); ¹H NMR (500 MHz, CDCl₃): δ = 3.83 (s, 6H), 3.96 (s, 3H), 6.53 (d, J = 16.0 Hz, 2H), 7.70 (d, J = 16.0 Hz, 2H), 7.79 (s, 1H), 8.20 ppm (s, 2H); ¹³C NMR (125 MHz, CDCl₃): δ = 51.9, 52.6, 120.1, 130.0, 131.5, 131.7, 135.6, 142.8, 165.9, 166.8 ppm; IR (KBr pellet): ν̄ = 1735 (s), 1712 (s), 1643 (s), 1597 (w), 1445 (s), 1346 (m), 1315 (m), 1290 (m), 1254 (s), 1173 (s), 1024 (w), 1003 (m), 920 (w), 860 (m), 769 (m), 666 (w), 562 cm⁻¹ (w).

Synthesis of 3,3'-(5-carboxy-1,3-phenylene)diacrylic acid (H₃L2): Me₃L2 (3.0 g, 10 mmol) and KOH (210 mmol, 11.7 g) in THF (50 mL) and H₂O (50 mL) were heated at 60 °C for 12 h. After the mixture was cooled down to room temperature, THF was evaporated under reduced pressure. The pH value of the mixture was adjusted to 1 by using concentrated

HCl. The precipitate was collected by filtration, washed with water several times, and dried at 50 °C to afford a white powder. Yield: 2.5 g (95%); ¹H NMR (500 MHz, [D₆]DMSO): δ = 6.74 (d, J = 16.0 Hz, 2H), 7.65 (d, J = 16.0 Hz, 2H), 8.16 (s, 2H), 8.35 ppm (s, 1H); ¹³C NMR (125 MHz, [D₆]DMSO): δ = 121.4, 130.2, 130.4, 133.1, 135.3, 142.3, 166.7, 167.4 ppm; IR (KBr pellet): ν̄ = 1724 (s), 1703 (s), 1637 (s), 1557 (w), 1442 (m), 1408 (m), 1293 (m), 1254 (m), 1216 (s), 981 (s), 863 (m), 773 (m), 691 (w), 616 (w), 581 cm⁻¹ (w).

Synthesis of [Cu₃(L1)₂(H₂O)₃]-2DMF-5.5H₂O (ZJU-35): H₃L1 (20 mg, 0.085 mmol), Cu(NO₃)₂·3H₂O (40 mg, 0.17 mmol), 0.1 M HCl (2.8 mL), DMF (20 mL), and H₂O (12 mL) were mixed and heated at 65 °C for two days. Blue crystals of ZJU-35 were collected by filtration, washed with EtOH and Et₂O, and dried in air. Yield: 75%; IR (KBr pellet): ν̄ = 1652 (s), 1614 (m), 1560 (m), 1497 (w), 1440 (m), 1378 (s), 1262 (m), 1107 (w), 984 (w), 874 (w), 777 (m), 730 (m), 628 cm⁻¹ (w); elemental analysis calcd (%) for C₂₈H₄₁N₂Cu₃O_{22.5}: C 35.17, H 4.32, N 2.93; found: C 35.13, H 4.15, N 2.87

Synthesis of [Cu₃(L2)₂(H₂O)₃]-5DMF-6.5H₂O (ZJU-36): H₃L2 (20 mg, 0.076 mmol), Cu(NO₃)₂·3H₂O (40 mg, 0.17 mmol), 0.1 M HCl (5.4 mL), DMF (20 mL), and H₂O (4 mL) were mixed and heated at 65 °C for two days. Blue crystals of ZJU-36 were collected by filtration, washed with EtOH and Et₂O, and dried in air. Yield: 79%; IR (KBr pellet): ν̄ = 1652 (s), 1588 (m), 1497 (w), 1437 (m), 1397 (s), 1282 (m), 1165 (w), 1101 (m), 984 (m), 870 (m), 789 (m), 754 (w), 665 (w), 611 cm⁻¹ (w); elemental analysis calcd (%) for C₄₁H₆₈N₃Cu₃O_{26.5}: C 39.53, H 5.50, N 5.62; found: C 39.43, H 5.59, N 5.79.

Crystal data for ZJU-35: C₂₂H₁₆Cu₃O₁₅, M_r = 710.97, cubic, Fm $\bar{3}$ m, a = 29.8307(6) Å, V = 26545.5(9) Å³, Z = 16, T = 293 K, ρ_{calcd} = 0.712 g cm⁻³, μ = 1.384 mm⁻¹, F(000) = 5680, 8749 reflections, 999 independent reflections, R_{int} = 0.0294, R₁[I > 2σ(I)] = 0.0783, wR₂ = 0.2318, GOF = 1.003.

Crystal data for ZJU-36: C₂₆H₂₀Cu₃O₁₅, M_r = 763.04, cubic, Fm $\bar{3}$ m, a = 33.6167(7) Å, V = 37989.6(14) Å³, Z = 16, T = 293 K, ρ_{calcd} = 0.534 g cm⁻³, μ = 0.982 mm⁻¹, F(000) = 6128, 7843 reflections, 1367 independent reflections, R_{int} = 0.0783, R₁[I > 2σ(I)] = 0.0682, wR₂ = 0.1560, GOF = 1.037.

CCDC-898168 (ZJU-35) and -900115 (ZJU-36) contain the supplementary crystallographic data for this paper. These data can be obtained free of charge from the Cambridge Crystallographic Data Centre via www.ccdc.cam.ac.uk/data_request/cif.

Acknowledgements

This work was supported by the National Natural Science Foundation of China (grant nos. 21073158 and J1210042), Zhejiang Provincial Natural Science Foundation of China (grant no. Z4100038), the Fundamental Research Funds for the Central Universities (grant no. 2013FZA3006) and Welch Foundation AX-1730 (B.C.), and partially supported by DOE-BES grant no. DE-FG02-08ER46522 (T.Y.). We thank Michael O'Keefe for the very constructive discussions.

- [1] J. R. Long, O. M. Yaghi, *Chem. Soc. Rev.* **2009**, *38*, 1213.
- [2] H.-C. Zhou, J. R. Long, O. M. Yaghi, *Chem. Rev.* **2012**, *112*, 673.
- [3] S. A. Allison, R. M. Barrer, *J. Chem. Soc. A* **1969**, 1717.
- [4] B. F. Hoskins, R. Robson, *J. Am. Chem. Soc.* **1989**, *111*, 5962.
- [5] a) M. Kondo, T. Yoshitomi, K. Seki, H. Matsuzaka, S. Kitagawa, *Angew. Chem.* **1997**, *109*, 1844; *Angew. Chem. Int. Ed. Engl.* **1997**, *36*, 1725; b) H. Li, M. Eddaoudi, T. L. Groy, O. M. Yaghi, *J. Am. Chem. Soc.* **1998**, *120*, 8571; c) H. Li, M. O'Keefe, M. Eddaoudi, M. O. M. Yaghi, *Nature* **1999**, *402*, 276; d) S. S.-Y. Chui, S. M.-F. Lo, J. P. H. Charmant, A. G. Orpen, I. D. Williams, *Science* **1999**, *283*, 1148.
- [6] a) B. F. Abrahams, B. F. Hoskins, D. M. Michail, R. Robson, *Nature* **1994**, *369*, 727; b) S. Subramanian, M. J. Zaworotko, *Angew. Chem.* **1995**, *107*, 2295; *Angew. Chem. Int. Ed. Engl.* **1995**, *34*, 2127; c) G. B.

- Gardner, D. Venkataraman, J. S. Moore, S. Lee, *Nature* **1995**, *374*, 792; d) O. M. Yaghi, G. Li, H. Li, *Nature* **1995**, *378*, 703.
- [7] a) S. Kitagawa, R. Kitaura, S. Noro, *Angew. Chem.* **2004**, *116*, 2388; *Angew. Chem. Int. Ed.* **2004**, *43*, 2334; b) D. Bradshaw, J. B. Claridge, E. J. Cussen, T. J. Prior, M. J. Rosseinsky, *Acc. Chem. Res.* **2005**, *38*, 273; c) X. Zhao, B. Xiao, A. J. Fletcher, K. Thomas, D. Bradshaw, M. J. Rosseinsky, *Science* **2004**, *306*, 1012; d) B. Chen, S.-C. Xiang, G.-D. Qian, *Acc. Chem. Res.* **2010**, *43*, 1115; e) S. R. Caskey, A. G. Wong-Foy, A. J. Matzger, *J. Am. Chem. Soc.* **2008**, *130*, 10870; f) J. Zhang, T. Wu, S.-M. Chen, P. Feng, X. Bu, *Angew. Chem.* **2009**, *121*, 3538; *Angew. Chem. Int. Ed.* **2009**, *48*, 3486; g) J.-P. Zhang, X.-M. Chen, *J. Am. Chem. Soc.* **2009**, *131*, 5516; h) Y.-B. Zhang, W.-X. Zhang, F.-Y. Feng, J.-P. Zhang, X.-M. Chen, *Angew. Chem.* **2009**, *121*, 5391; *Angew. Chem. Int. Ed.* **2009**, *48*, 5287; i) Q. Lin, T. Wu, S.-T. Zheng, X. Bu, P. Feng, *J. Am. Chem. Soc.* **2012**, *134*, 784; j) H.-L. Jiang, Q. Xu, *Chem. Commun.* **2011**, *47*, 3351; k) Y. K. Park, S. B. Choi, H. Kim, K. Kim, B.-H. Won, K. Choi, J.-S. Choi, W.-S. Ahn, N. Won, S. Kim, D. H. Jung, S.-H. Choi, G.-H. Kim, S.-S. Cha, Y. H. Jhon, J. K. Yang, J. Kim, *Angew. Chem.* **2007**, *119*, 8378; *Angew. Chem. Int. Ed.* **2007**, *46*, 8230; l) G. Férey, C. Serre, T. Devic, G. Maurin, H. Jobic, P. L. Llewellyn, G. De Weireld, A. Vimont, M. Daturi, J.-S. Chang, *Chem. Soc. Rev.* **2011**, *40*, 550; m) G. Férey, *Chem. Soc. Rev.* **2008**, *37*, 191; n) J. An, O. K. Farha, J. T. Hupp, E. Pohl, J. I. Yeh, N. L. Rosi, *Nat. Commun.* **2012**, *3*, 604; o) S.-T. Zheng, T. Wu, C. Chou, A. Fuhr, P. Feng, X. Bu, *J. Am. Chem. Soc.* **2012**, *134*, 4517; p) Y. He, W. Zhou, R. Krishna, B. Chen, *Chem. Commun.* **2012**, *48*, 11813; q) T. A. Makal, J.-R. Li, W. Lu, H.-C. Zhou, *Chem. Soc. Rev.* **2012**, *41*, 7761; r) W. Zhou, *Chem. Rec.* **2010**, *10*, 200; s) K. Konstas, T. Osl, Y. Yang, M. Batten, N. Burke, A. J. Hill, M. R. Hilla, *J. Mater. Chem.* **2012**, *22*, 16698; t) S. Ma, H.-C. Zhou, *Chem. Commun.* **2010**, *46*, 44; u) X. Lin, N. R. Champness, M. Schröder, *Top. Curr. Chem.* **2009**, *293*, 35; v) K. C. Stylianou, J. Rabone, S. Y. Chong, R. Heck, J. Armstrong, P. V. Wiper, K. E. Jelfs, S. Zlatogorsky, J. Bacsá, A. G. McLennan, C. P. Ireland, Y. Z. Khimyak, K. M. Thomas, D. Bradshaw, M. J. Rosseinsky, *J. Am. Chem. Soc.* **2012**, *134*, 20466.
- [8] a) J.-R. Li, R. J. Kuppler, H.-C. Zhou, *Chem. Soc. Rev.* **2009**, *38*, 1477; b) H. Wu, Q. Gong, D. H. Olson, J. Li, *Chem. Rev.* **2012**, *112*, 836; c) H. Deng, C. J. Doonan, H. Furukawa, R. B. Ferreira, J. Towne, C. B. Knobler, B. Wang, O. M. Yaghi, *Science* **2010**, *327*, 846; d) S. Xiang, Z. Zhang, C.-G. Zhao, K. Hong, X. Zhao, D.-R. Ding, M.-H. Xie, C.-D. Wu, M. C. Das, R. Gill, K. M. Thomas, B. Chen, *Nat. Commun.* **2011**, *2*, 204; e) P. Nugent, Y. Belmabkhout, S. D. Burd, A. J. Cairns, R. Luebke, K. Forrester, T. Pham, S. Ma, B. Space, L. Wojtas, E. Mohamed, M. J. Zaworotko, *Nature* **2013**, *495*, 80; f) A. J. Lan, K. H. Li, H. H. Wu, D. H. Olson, T. J. Emge, W. Ki, M. C. Hong, J. Li, *Angew. Chem.* **2009**, *121*, 2370; *Angew. Chem. Int. Ed.* **2009**, *48*, 2334; g) Z. Xie, L. Ma, K. E. de Krafft, A. Jin, W. Lin, *J. Am. Chem. Soc.* **2010**, *132*, 922; h) B. Chen, C. Liang, J. Yang, D. S. Contreras, Y. L. Clancy, E. B. Lobkovsky, O. M. Yaghi, S. Dai, *Angew. Chem.* **2006**, *118*, 1418; *Angew. Chem. Int. Ed.* **2006**, *45*, 1390; i) R. Vaidhyanathan, S. S. Iremonger, G. K. H. Shimizu, P. G. Boyd, S. Alavi, T. K. Woo, *Science* **2010**, *330*, 650; j) J. M. Taylor, K. W. Dawson, G. K. H. Shimizu, *J. Am. Chem. Soc.* **2013**, *135*, 1193; k) S. Kim, K. W. Dawson, B. S. Gelfand, J. M. Taylor, G. K. H. Shimizu, *J. Am. Chem. Soc.* **2013**, *135*, 963; l) J. M. Taylor, R. Vaidhyanathan, S. S. Iremonger, G. K. H. Shimizu, *J. Am. Chem. Soc.* **2012**, *134*, 14338; m) N. Yanai, K. Kitayama, Y. Hijikata, H. Sato, R. Matsuda, Y. Kubota, M. Takata, M. Mizuno, T. Uemura, S. Kitagawa, *Nat. Mater.* **2011**, *10*, 787; n) X.-S. Wang, L. Meng, Q. Cheng, C. Kim, L. Wojtas, M. Chrzanowski, Y.-S. Chen, X. P. Zhang, S. Ma, *J. Am. Chem. Soc.* **2011**, *133*, 16322.
- [9] a) J. S. Seo, D. Whang, H. Lee, S. I. Jun, J. Oh, Y. J. Jeon, K. Kim, *Nature* **2000**, *404*, 982; b) C.-D. Wu, A. Hu, L. Zhang, W. Lin, *J. Am. Chem. Soc.* **2005**, *127*, 8940; c) L. Ma, C. Abney, W. Lin, *Chem. Soc. Rev.* **2009**, *38*, 1248; d) J. Lee, O. K. Farha, J. Roberts, K. A. Scheidt, S. T. Nguyen, J. T. Hupp, *Chem. Soc. Rev.* **2009**, *38*, 1450; e) A. Corma, L. García, H. F. X. Xamena, *Chem. Rev.* **2010**, *110*, 4606; f) P. Wu, C. He, J. Wang, X. Peng, X. Li, Y. An, C. Duan, *J. Am. Chem. Soc.* **2012**, *134*, 14991; g) G.-Q. Kong, S. Ou, C. Zou, C.-D. Wu, *J. Am. Chem. Soc.* **2012**, *134*, 19851; h) A. Aijaz, A. Karkamkar, Y. J. Choi, N. Tsumori, E. Rönnebro, T. Autrey, H. Shioyama, Q. Xu, *J. Am. Chem. Soc.* **2012**, *134*, 13926; i) S. Shimomura, M. Higuchi, R. Matsuda, K. Yoneda, Y. Hijikata, Y. Kubota, Y. Mita, J. Kim, M. Takata, S. Kitagawa, *Nat. Chem.* **2010**, *2*, 633; j) H. Sato, R. Matsuda, K. Sugimoto, M. Takata, S. Kitagawa, *Nat. Mater.* **2010**, *9*, 661; k) S. Horike, S. Shimomura, S. Kitagawa, *Nat. Chem.* **2009**, *1*, 695; l) L. Meng, Q. Cheng, C. Kim, W.-Y. Gao, L. Wojtas, Y.-S. Cheng, M. J. Zaworotko, X. P. Zhang, S. Ma, *Angew. Chem.* **2012**, *124*, 10229; *Angew. Chem. Int. Ed.* **2012**, *51*, 10082; m) V. Lykourinou, Y. Chen, X.-S. Wang, L. Meng, T. Hoang, L.-J. Ming, R. L. Musselman, S. Ma, *J. Am. Chem. Soc.* **2011**, *133*, 10382.
- [10] a) L. E. Kreno, K. Leong, O. K. Farha, M. Allendorf, R. P. Van Duyne, J. T. Hupp, *Chem. Rev.* **2012**, *112*, 1105; b) Y. Cui, Y. Yue, G. Qian, B. Chen, *Chem. Rev.* **2012**, *112*, 1126; c) H.-L. Jiang, Y. Tatsu, Z.-H. Lu, Q. Xu, *J. Am. Chem. Soc.* **2010**, *132*, 5586; d) Y.-Q. Lan, H.-L. Jiang, S.-L. Li, Q. Xu, *Adv. Mater.* **2011**, *23*, 5015; e) Y. Ikezoe, G. Washino, T. Uemura, S. Kitagawa, H. Matsui, *Nat. Mater.* **2012**, *11*, 1081; f) S. C. Sahoo, T. Kundu, R. Banerjee, *J. Am. Chem. Soc.* **2011**, *133*, 17950; g) R. Banerjee, H. Furukawa, D. Britt, C. Knobler, M. O'Keeffe, O. M. Yaghi, *J. Am. Chem. Soc.* **2009**, *131*, 3875; h) K. Sumida, D. L. Rogow, J. A. Mason, T. M. McDonald, E. D. Bloch, Z. R. Herm, T.-H. Bae, J. R. Long, *Chem. Rev.* **2012**, *112*, 724; i) X. Kong, E. Scott, W. Ding, J. A. Mason, J. R. Long, J. A. Reimer, *J. Am. Chem. Soc.* **2012**, *134*, 14341.
- [11] a) P. Horcajada, T. Chalati, C. Serre, B. Gillet, C. Sebrie, T. Baati, J. F. Marsaud, D. Eubank, P. Heurtaux, C. Clayette, J.-S. Kreuz, Y. K. Chang, V. Hwang, P.-N. Bories, L. Cynober, S. Gil, G. Férey, P. Couvreur, R. Gref, *Nat. Mater.* **2010**, *9*, 172; b) K. Gedrich, I. Senkowska, N. Klein, U. Stoeck, A. Henschel, M. R. Lohe, I. Baburin, A. Mueller, U. S. Kaskel, *Angew. Chem.* **2010**, *122*, 8667; *Angew. Chem. Int. Ed.* **2010**, *49*, 8489; c) J. An, S. J. Geib, N. L. Rosi, *J. Am. Chem. Soc.* **2010**, *132*, 38; d) E. Q. Procopio, F. Linares, C. Montoro, V. Colombo, A. Maspero, E. Barea, J. A. R. Navarro, *Angew. Chem.* **2010**, *122*, 7466; *Angew. Chem. Int. Ed.* **2010**, *49*, 7308; e) Y.-S. Bae, R. Q. Snurr, *Angew. Chem.* **2011**, *123*, 11790; *Angew. Chem. Int. Ed.* **2011**, *50*, 11586; g) S. Kaskel, R. Fischer, *J. Mater. Chem.* **2012**, *22*, 10093.
- [12] a) M. Eddaoudi, D. B. Moler, H. Li, B. Chen, T. M. Reineke, M. O'Keeffe, O. M. Yaghi, *Acc. Chem. Res.* **2001**, *34*, 319; b) G. Férey, C. Mellot-Draznieks, C. Serre, F. Millange, *Acc. Chem. Res.* **2005**, *38*, 217; c) O. M. Yaghi, M. O'Keeffe, N. Ockwig, H. K. Chae, M. Eddaoudi, J. Kim, *Nature* **2003**, *423*, 705; d) M. O'Keeffe, O. M. Yaghi, *Chem. Rev.* **2012**, *112*, 675.
- [13] M. Eddaoudi, J. Kim, N. Rosi, D. Vodak, J. Wachter, M. O'Keeffe, O. M. Yaghi, *Science* **2002**, *295*, 469.
- [14] H. K. Chae, D. Y. Siberio-Pérez, J. Kim, Y. Go, M. Eddaoudi, A. J. Matzger, M. O'Keeffe, O. M. Yaghi, *Nature* **2004**, *427*, 523.
- [15] a) K. Koh, A. G. Wong-Foy, A. J. Matzger, *J. Am. Chem. Soc.* **2009**, *131*, 4184; b) M. Padmanaban, P. Müller, C. Lieder, K. Gedrich, R. Grunker, V. Bon, I. Senkowska, S. Baumgärtner, S. Opelt, S. Paasch, E. Brunner, F. Glorius, E. Klemm, S. Kaskel, *Chem. Commun.* **2011**, *47*, 12089.
- [16] H. Furukawa, N. Ko, Y. B. Go, N. Aratani, S. B. Choi, E. Choi, A. Ö. Yazaydin, R. Q. Snurr, M. O'Keeffe, J. Kim, O. M. Yaghi, *Science* **2010**, *329*, 424.
- [17] a) M. Eddaoudi, J. Kim, D. Vodak, A. Sudik, J. Wachter, M. O'Keeffe, O. M. Yaghi, *Proc. Natl. Acad. Sci. USA* **2002**, *99*, 4900; b) S. A. Bourne, J. Lu, A. Mondal, B. Moulton, M. J. Zaworotko, B. Moulton, *Angew. Chem.* **2001**, *113*, 2169; *Angew. Chem. Int. Ed.* **2001**, *40*, 2111; c) B. Moulton, J. Lu, R. Hajndl, S. Hariharan, M. J. Zaworotko, *Angew. Chem.* **2002**, *114*, 2945; *Angew. Chem. Int. Ed.* **2002**, *41*, 2821.
- [18] a) M. Eddaoudi, J. Kim, M. O'Keeffe, O. M. Yaghi, *J. Am. Chem. Soc.* **2002**, *124*, 376; b) Z. Zhang, L. Wojtas, M. J. Zaworotko, *Cryst. Growth Des.* **2011**, *11*, 1441.
- [19] B. Chen, M. Eddaoudi, T. M. Reineke, J. Kampf, M. O'Keeffe, O. M. Yaghi, *J. Am. Chem. Soc.* **2000**, *122*, 11559.

- [20] B. Chen, M. Eddaoudi, S. T. Hyde, M. O'Keeffe, O. M. Yaghi, *Science* **2001**, *291*, 1021.
- [21] D. Sun, S. Ma, Y. Ke, D. J. Collins, H.-C. Zhou, *J. Am. Chem. Soc.* **2006**, *128*, 3896.
- [22] a) Y. Yan, I. Telepeni, S. Yang, X. Lin, W. Kockelmann, A. Dailly, A. J. Blake, W. Lewis, G. S. Walker, D. R. Allan, S. A. Barnett, N. R. Champness, M. Schroder, *J. Am. Chem. Soc.* **2010**, *132*, 4092; b) O. K. Farha, C. E. Wilmer, I. Eryazici, B. G. Hauser, P. A. Parilla, K. O'Neill, A. A. Sarjeant, S. T. Nguyen, R. Q. Snurr, J. T. Hupp, *J. Am. Chem. Soc.* **2012**, *134*, 9860; c) L. Ma, J. M. Falkowski, C. Abney, W. Lin, *Nat. Chem.* **2010**, *2*, 838; d) F. Nouar, J. F. Eubank, T. Bousquet, L. Wojtas, M. J. Zaworotko, M. Eddaoudi, *J. Am. Chem. Soc.* **2008**, *130*, 1833; e) J. J. Perry IV, V. Ch. Kravtsov, G. J. McManus, M. J. Zaworotko, *J. Am. Chem. Soc.* **2007**, *129*, 10076; f) J. K. Schnobrich, O. Lebel, K. A. Cychosz, A. Dailly, A. G. Wong-Foy, A. J. Matzger, *J. Am. Chem. Soc.* **2010**, *132*, 13941; g) L. Ma, D. J. Mihalcik, W. Lin, *J. Am. Chem. Soc.* **2009**, *131*, 4610; h) S. Ma, D. Sun, J. M. Simmons, C. D. Collier, D. Yuan, H.-C. Zhou, *J. Am. Chem. Soc.* **2008**, *130*, 1012; i) W. Lu, D. Yuan, T. A. Makal, J.-R. Li, H.-C. Zhou, *Angew. Chem.* **2012**, *124*, 1612; *Angew. Chem. Int. Ed.* **2012**, *51*, 1580; j) Y. Yan, X. Lin, S. Yang, A. J. Blake, A. Dailly, N. R. Champness, P. Hubberstey, M. Schröder, *Chem. Commun.* **2009**, 1025; k) Y. Yan, S. Yang, A. J. Blake, W. Lewis, E. Poirier, S. A. Barnett, N. R. Champness, M. Schröder, *Chem. Commun.* **2011**, *47*, 9995; l) Y. Yan, A. Blake, J. Lewis, S. A. Barnett, A. Dailly, N. R. Champness, M. Schroder, *Chem. Eur. J.* **2011**, *17*, 11162; m) Y. Zou, M. Park, S. Hong, M. S. Lah, *Chem. Commun.* **2008**, 2340.
- [23] H. Furukawa, Y. B. Go, N. Y. Ko, K. Park, F. J. Uribe-Romo, J. Kim, M. O'Keeffe, O. M. Yaghi, *Inorg. Chem.* **2011**, *50*, 9147.
- [24] a) B. Chen, N. W. Ockwig, A. R. Millward, D. S. Contreras, O. M. Yaghi, *Angew. Chem.* **2005**, *117*, 4823; *Angew. Chem. Int. Ed.* **2005**, *44*, 4745; b) X. Lin, J. Jia, X. Zhao, K. M. Thomas, A. J. Blake, G. S. Walker, N. R. Champness, P. Hubberstey, M. Schroder, *Angew. Chem.* **2006**, *118*, 7518; *Angew. Chem. Int. Ed.* **2006**, *45*, 7358.
- [25] O. K. Farha, I. Eryazici, N. C. Jeong, B. G. Hauser, C. E. Wilmer, A. A. Sarjeant, R. Q. Snurr, S. T. Nguyen, A. O. Yazaydin, J. T. Hupp, *J. Am. Chem. Soc.* **2012**, *134*, 15016.
- [26] X.-S. Wang, S. Ma, D. Yuan, J. W. Yoon, Y. K. Hwang, J.-S. Chang, X. Wang, M. R. Jorgensen, Y. S. Chen, H.-C. Zhou, *Inorg. Chem.* **2009**, *48*, 7519.
- [27] A. L. Spek, *PLATON, a multipurpose crystallographic tool*, Utrecht University, Utrecht, The Netherlands, **2008**.
- [28] U. Stoeck, S. Krause, V. Bon, I. Senkovska, S. Kaskel, *Chem. Commun.* **2012**, *48*, 10841.
- [29] P. D. C. Dietzel, V. Besikiotis, R. Blom, *J. Mater. Chem.* **2009**, *19*, 7362.
- [30] Y. He, W. Zhou, T. Yildirim, B. Chen, *Energy Environ. Sci.* **2013**, *6*, 2735.
- [31] C. E. Wilmer, O. K. Farha, T. Yildirim, I. Eryazici, V. Krungleviciute, A. A. Sarjeant, R. Q. Snurr, J. T. Hupp, *Energy Environ. Sci.* **2013**, *6*, 1158.
- [32] Y. Peng, G. Srinivas, C. E. Wilmer, R. Q. Snurr, J. T. Hupp, T. Yildirim, O. K. Farha, *Chem. Commun.* **2013**, *49*, 2992.
- [33] J. M. Simmons, H. Wu, W. Zhou, T. Yildirim, *Energy Environ. Sci.* **2011**, *4*, 2177.
- [34] P. L. Llewellyn, S. Bourrelly, C. Serre, A. Vimont, M. Daturi, L. Hamon, G. D. Weireld, J.-S. Chang, D.-Y. Hong, Y. K. Hwang, S. H. Jhung, G. Férey, *Langmuir* **2008**, *24*, 7245.
- [35] A. L. Myers, J. M. Prausnitz, *AIChE J.* **1965**, *11*, 121.
- [36] X. Duan, J. Yu, J. Cai, Y. He, C. Wu, W. Zhou, T. Yildirim, Z. Zhang, S. Xiang, M. O'Keeffe, B. Chen, G. Qian, *Chem. Commun.* **2013**, *49*, 2043.
- [37] Z. R. Herm, J. A. Swisher, B. Smit, R. Krishna, J. R. Long, *J. Am. Chem. Soc.* **2011**, *133*, 5664.
- [38] a) Z. R. Herm, R. Krishna, J. R. Long, *Microporous Mesoporous Mater.* **2012**, *157*, 94; b) Z. R. Herm, R. Krishna, J. R. Long, *Microporous Mesoporous Mater.* **2012**, *151*, 481; c) H. Wu, K. Yao, Y. Zhu, B. Li, Z. Shi, R. Krishna, J. Li, *J. Phys. Chem. C* **2012**, *116*, 16609.
- [39] a) E. D. Bloch, W. L. Queen, R. Krishna, J. M. Zadrozny, C. M. Brown, J. R. Long, *Science* **2012**, *335*, 1606; b) S. Xiang, Y. He, Z. Zhang, H. Wu, W. Zhou, R. Krishna, B. Chen, *Nat. Commun.* **2012**, *3*, 954; c) Y. He, R. Krishna, B. Chen, *Energy Environ. Sci.* **2012**, *5*, 9107.
- [40] For example, a) B. Xiao, P. S. Wheatley, X. Zhao, A. J. Fletcher, S. Fox, A. G. Rossi, I. L. Megson, S. Bordiga, L. Regli, K. M. Thomas, R. E. Morris, *J. Am. Chem. Soc.* **2007**, *129*, 1203; b) C.-Y. Sun, S.-X. Liu, D.-D. Liang, K.-Z. Shao, Y.-H. Ren, Z.-M. Su, *J. Am. Chem. Soc.* **2009**, *131*, 1883; c) H. Guo, G. Zhu, I. J. Hewitt, S. Qiu, *J. Am. Chem. Soc.* **2009**, *131*, 1646; d) V. K. Peterson, G. J. Kearley, Y. Wu, A. J. Ramirez-Cuesta, E. Kemner, C. J. Kepert, *Angew. Chem.* **2010**, *122*, 595; *Angew. Chem. Int. Ed.* **2010**, *49*, 585; e) Y.-N. Wu, F. Li, W. Zhu, J. Cui, C.-A. Tao, C. Lin, P. M. Hannam, G. Li, *Angew. Chem.* **2011**, *123*, 12726; *Angew. Chem. Int. Ed.* **2011**, *50*, 12518.

Received: June 29, 2013
Published online: September 23, 2013

CHEMISTRY

A EUROPEAN JOURNAL

Supporting Information

© Copyright Wiley-VCH Verlag GmbH & Co. KGaA, 69451 Weinheim, 2013

Expanded Organic Building Units for the Construction of Highly Porous Metal–Organic Frameworks

**Guo-Qiang Kong,^[a] Zhi-Da Han,^[a] Yabing He,^[b] Sha Ou,^[a] Wei Zhou,^[c, d]
Taner Yildirim,^[d, e] Rajamani Krishna,^{*,[f]} Chao Zou,^[a] Banglin Chen,^{*,[b]} and
Chuan-De Wu^{*,[a]}**

chem_201302515_sm_miscellaneous_information.pdf

Supporting Information for

Expanded Organic Building Units for the Construction of Highly Porous Metal-Organic Frameworks

Guo-Qiang Kong,^a Zhi-Da Han,^a Yabing He,^b Sha Ou,^a Wei Zhou,^c Taner Yildirim,^d Rajamani Krishna,^{e*} Chao Zou,^a Banglin Chen,^{b*} Chuan-De Wu^{a*}

^a*Center for Chemistry of High-Performance and Novel Materials, Department of Chemistry, Zhejiang University, Hangzhou 310027, P. R. China. E-mail: cdwu@zju.edu.cn*

^b*Department of Chemistry, University of Texas at San Antonio, One UTSA Circle, San Antonio, Texas 78249-0698, USA. E-mail: banglin.chen@utsa.edu*

^c*NIST Center for Neutron Research, Gaithersburg, Maryland 20899-6102, Department of Materials Science and Engineering, University of Maryland, College Park Maryland 20742, USA*

^d*NIST Center for Neutron Research, Gaithersburg, Maryland 20899-6102, Department of Materials Science and Engineering, University of Pennsylvania, Philadelphia, Pennsylvania 19104-6272, USA*

^e*Van't Hoff Institute of Molecular Science, University of Amsterdam, Science Park 904, 1098 XH Amsterdam, The Netherlands. E-mail: r.krishna@uva.nl*

Single crystal X-ray data collections and structure determinations.

The determinations of the unit cells and data collections for the crystals of **ZJU-35** and **ZJU-36** were performed on an Oxford Xcalibur Gemini Ultra diffractometer with an Atlas detector. The data were collected using graphite-monochromatic enhanced ultra Cu radiation ($\lambda = 1.54178 \text{ \AA}$) at 293 K. The data sets were corrected by empirical absorption correction using spherical harmonics, implemented in SCALE3 ABSPACK scaling algorithm.^{S1} The structures of the two compounds were solved by direct methods, and refined by full-matrix least-square methods with the **SHELX-97** program package.^{S2} The solvent molecules in the two compounds are highly disordered, SQUEEZE subroutine of the PLATON software suit was used to remove the scattering from the highly disordered guest molecules.^{S3} The resulting new files were used to further refine the structures. The H atoms on C atoms were generated geometrically.

Supporting Figures

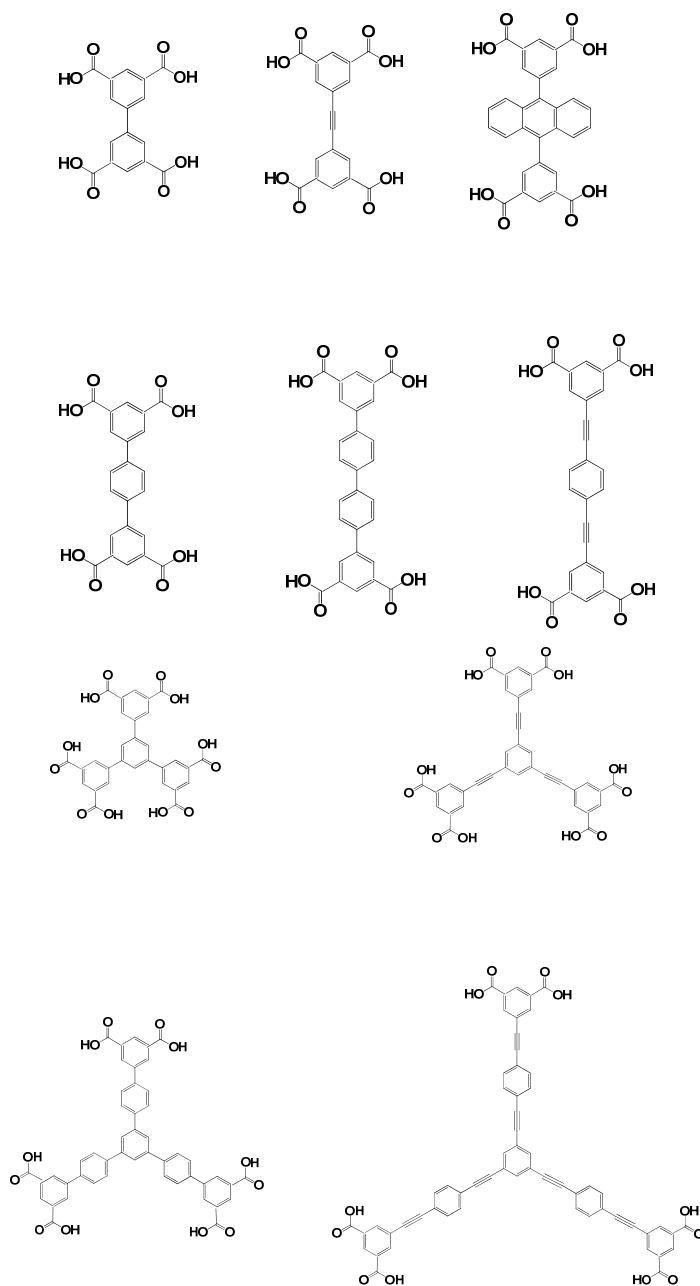


Figure S1. Some of the developed organic linkers based on *m*-benzenedicarboxylate for the construction of highly porous MOFs for gas storage and separation.

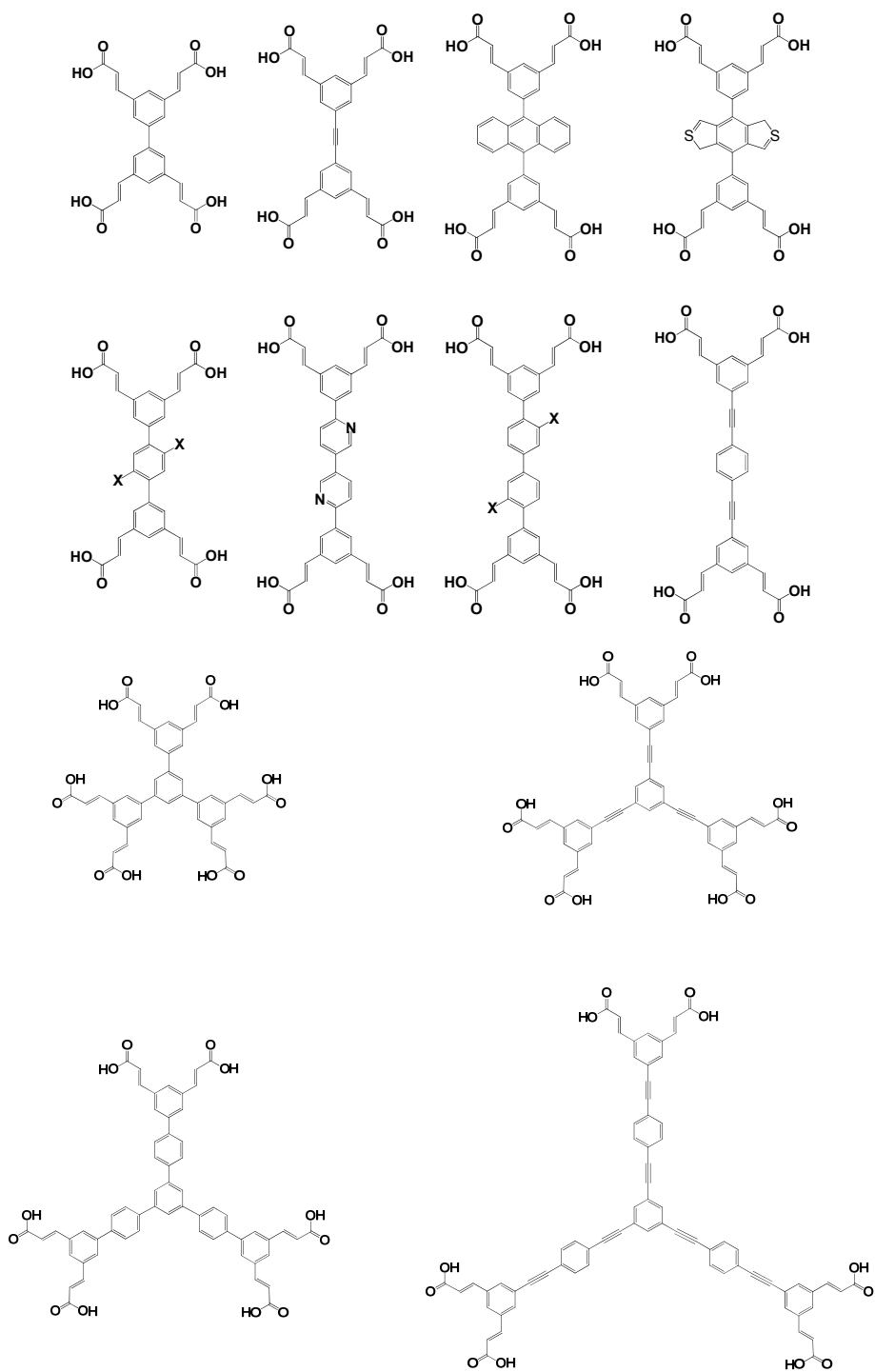


Figure S2. Some future developed organic linkers built from our new organic building units mentioned in the current manuscript for the construction of highly porous MOFs for gas storage and separation.

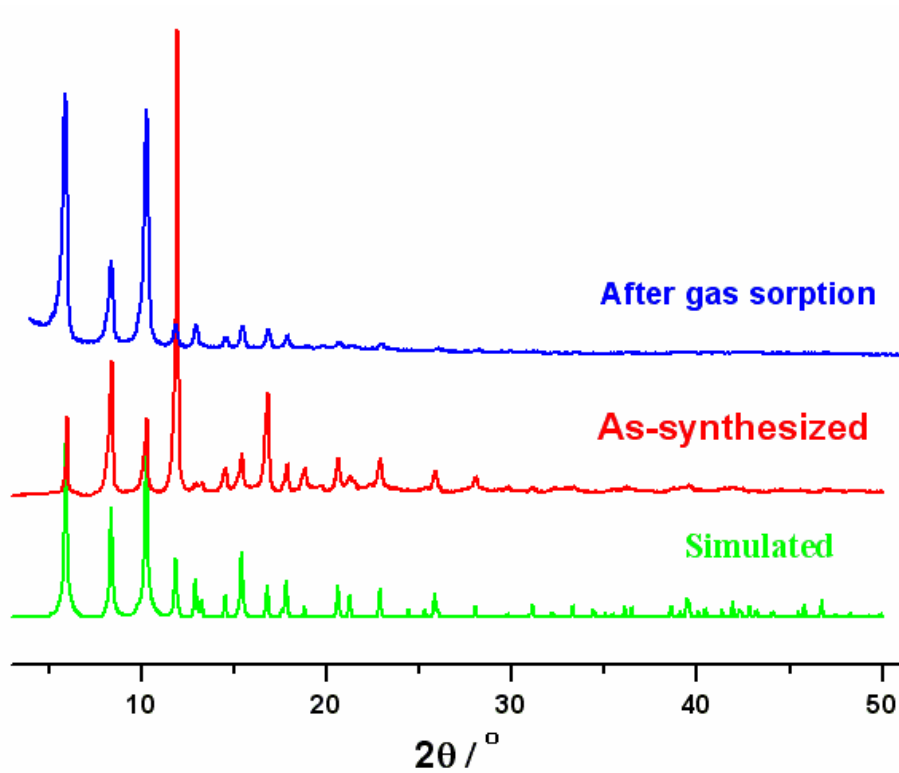


Figure S3. Powder X-ray diffraction patterns for **ZJU-35** (simulated from single crystal structure data (green), as-synthesized (red) and the one after gas sorption experiment).

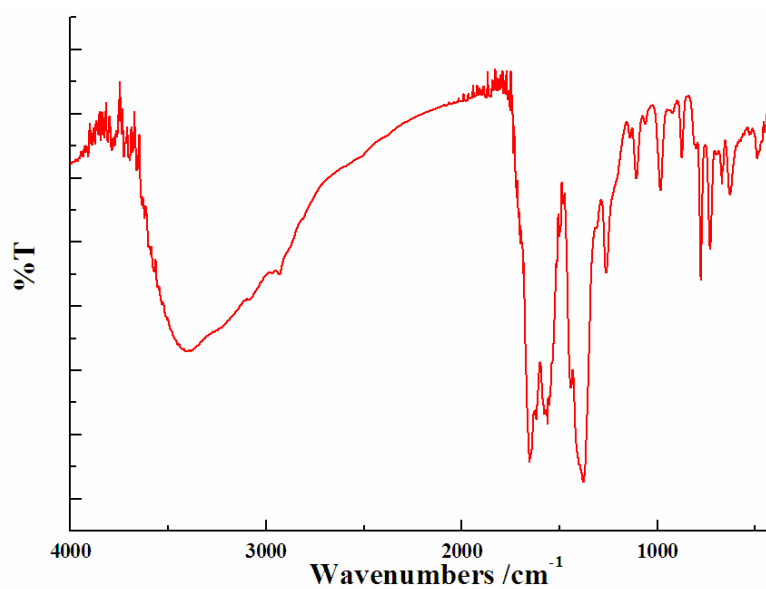


Figure S4. IR spectrum of the as-synthesized **ZJU-35**.

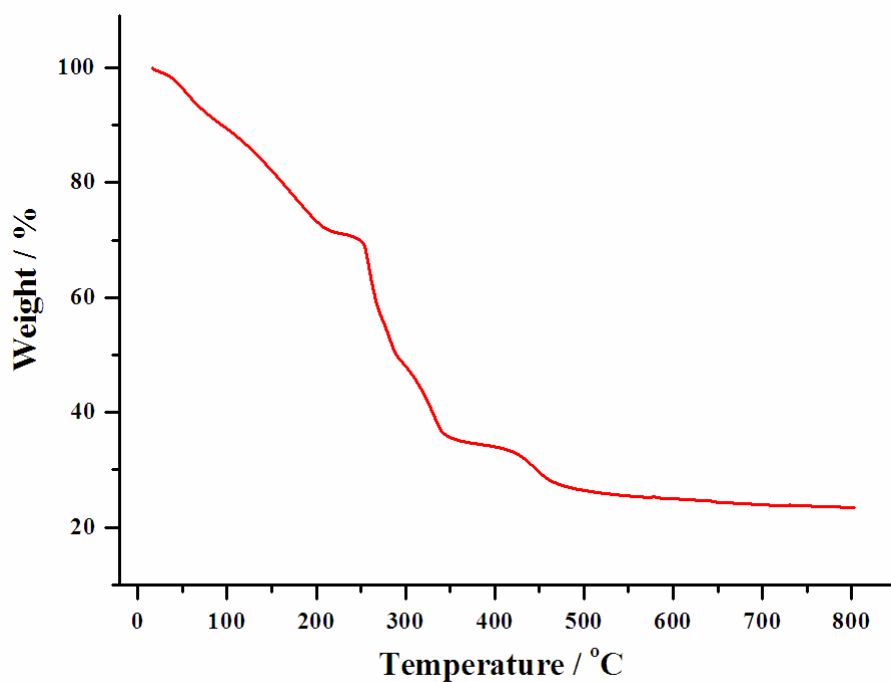


Figure S5. TGA graph of the as-synthesized ZJU-35.

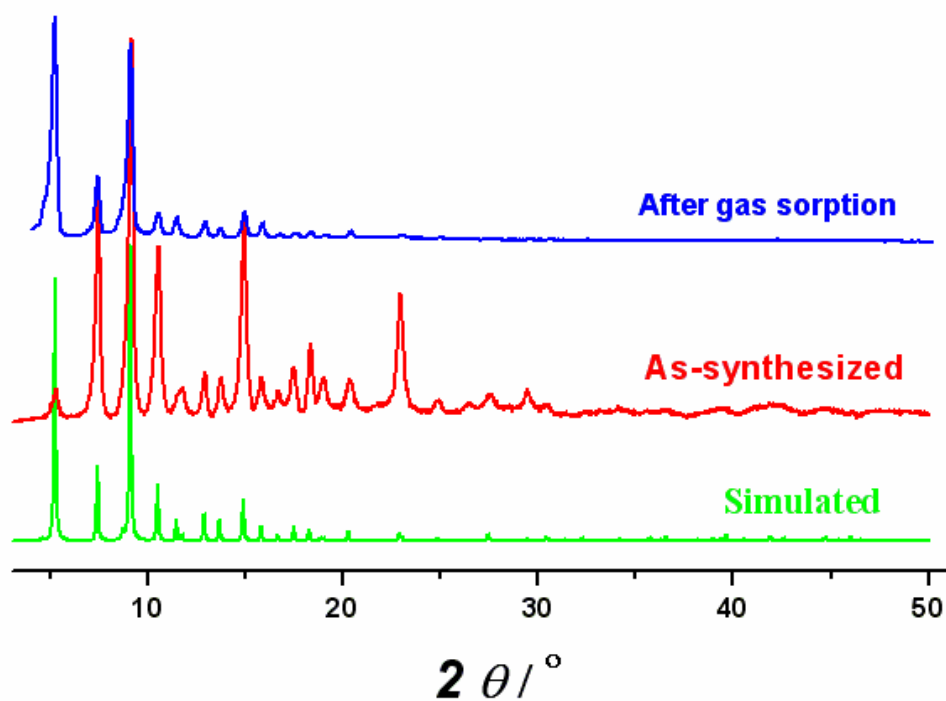


Figure S6. Powder X-ray diffraction patterns for ZJU-36 (simulated from single crystal structure data (green), as-synthesized (red) and the one after gas sorption experiment).

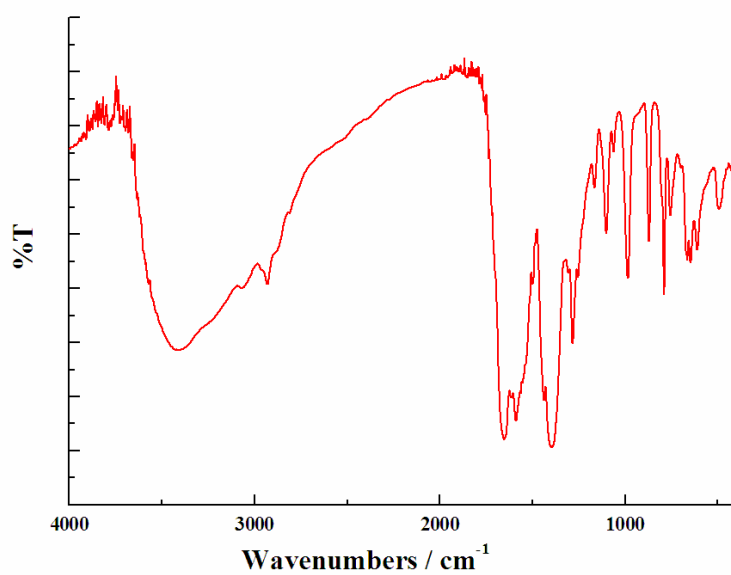


Figure S7. IR spectrum of the as-synthesized **ZJU-36**.

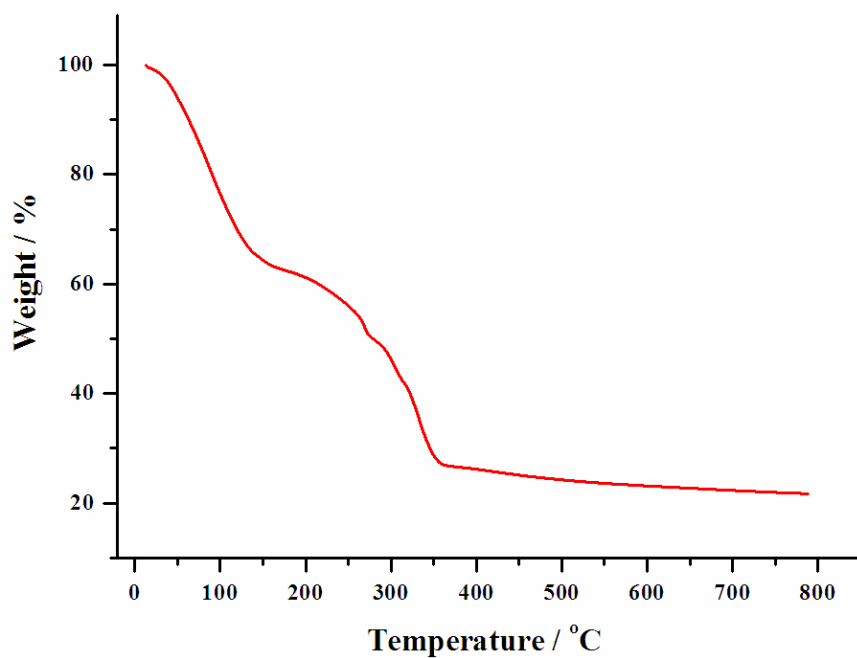


Figure S8. TGA graph of the as-synthesized **ZJU-36**.

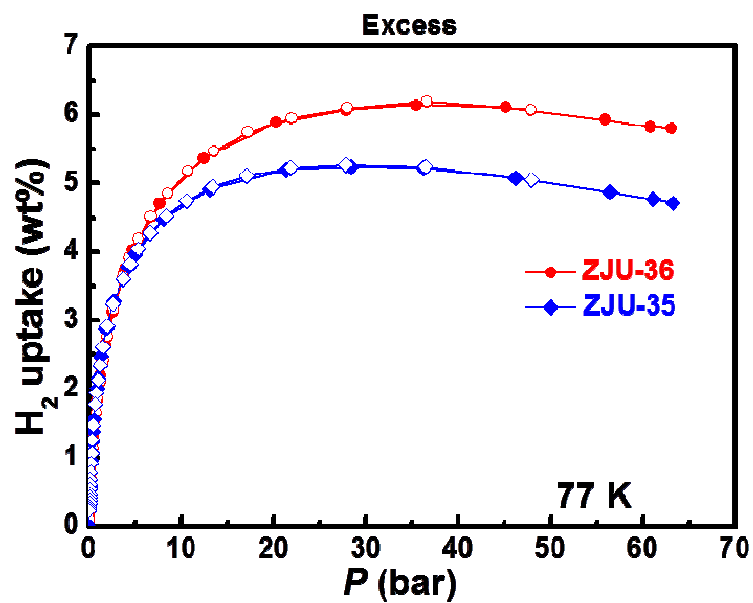


Figure S9. Excess H₂ sorption isotherms of ZJU-35 and ZJU-36 at 77 K.

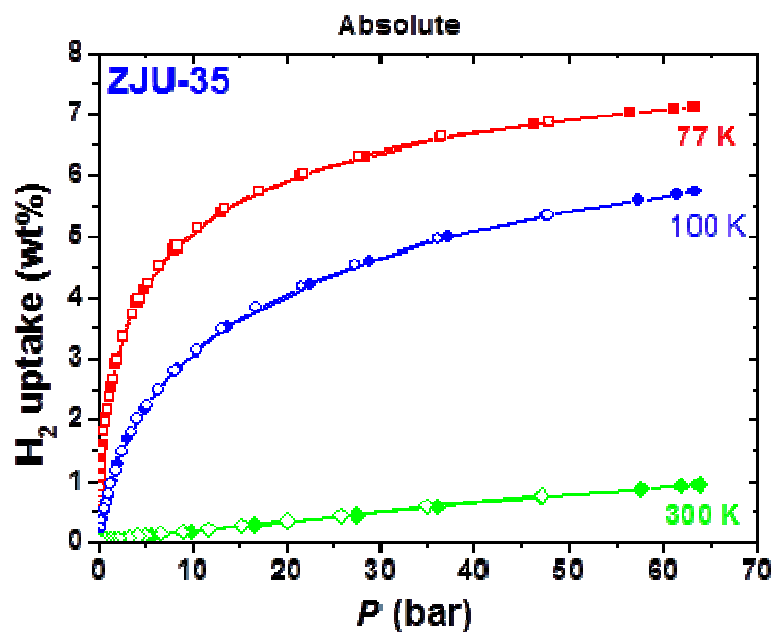


Figure S10. H₂ (absolute) sorption isotherms of ZJU-35 at different temperatures.

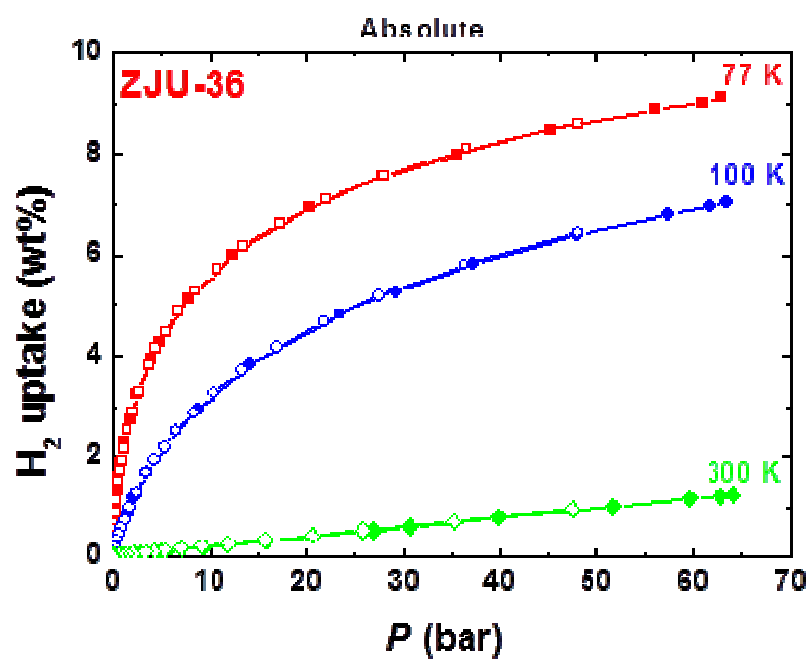


Figure S11. H₂ (absolute) sorption isotherms of ZJU-36 at different temperatures.

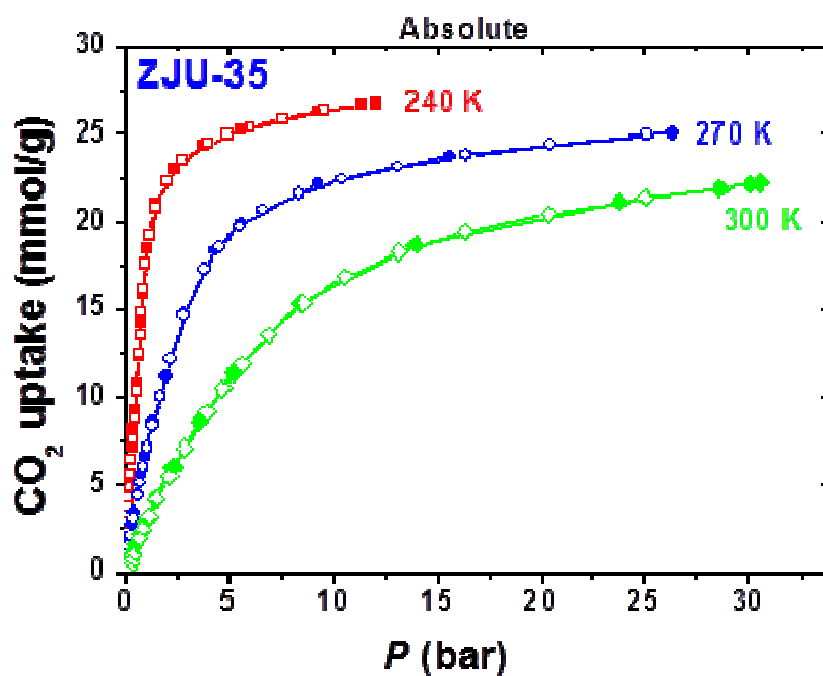


Figure S12. CO₂ (absolute) sorption isotherms of ZJU-35 at different temperatures.

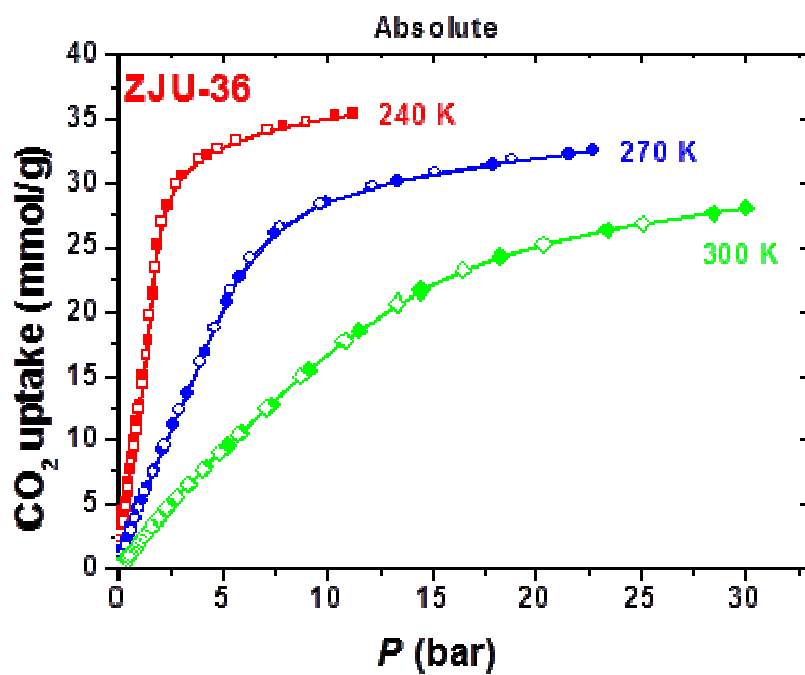


Figure S13. CO₂ (absolute) sorption isotherms of ZJU-36 at different temperatures.

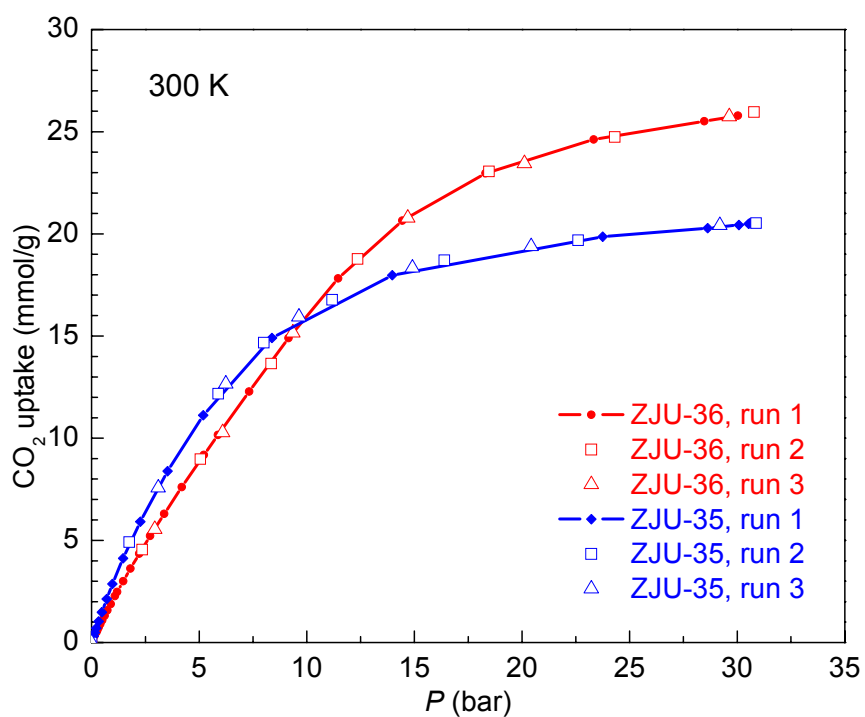


Figure S14. Excess CO₂ adsorption isotherms of ZJU-35 and ZJU-36 at 300 K. The gas uptake amount remains unchanged for the three cycles examined.

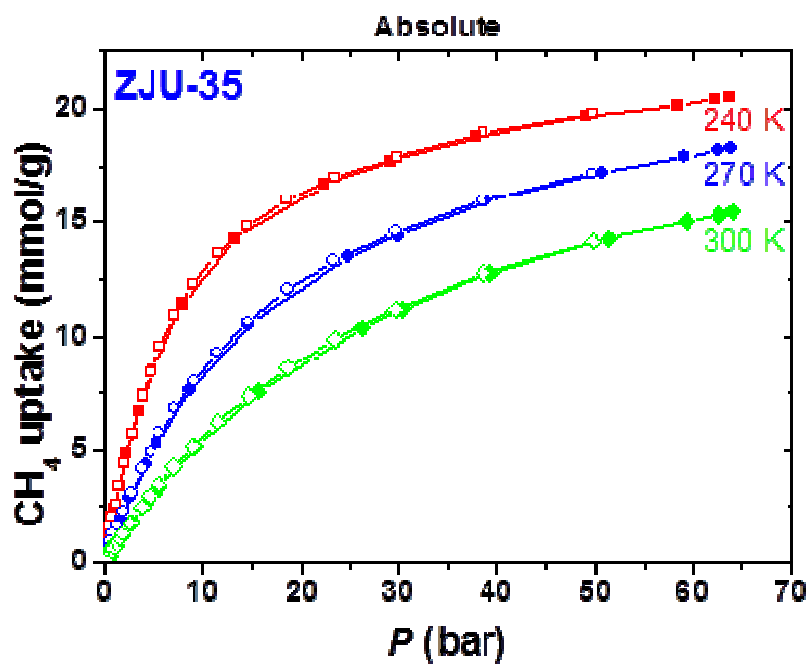


Figure S15. CH₄ (absolute) sorption isotherms of ZJU-35 at different temperatures.

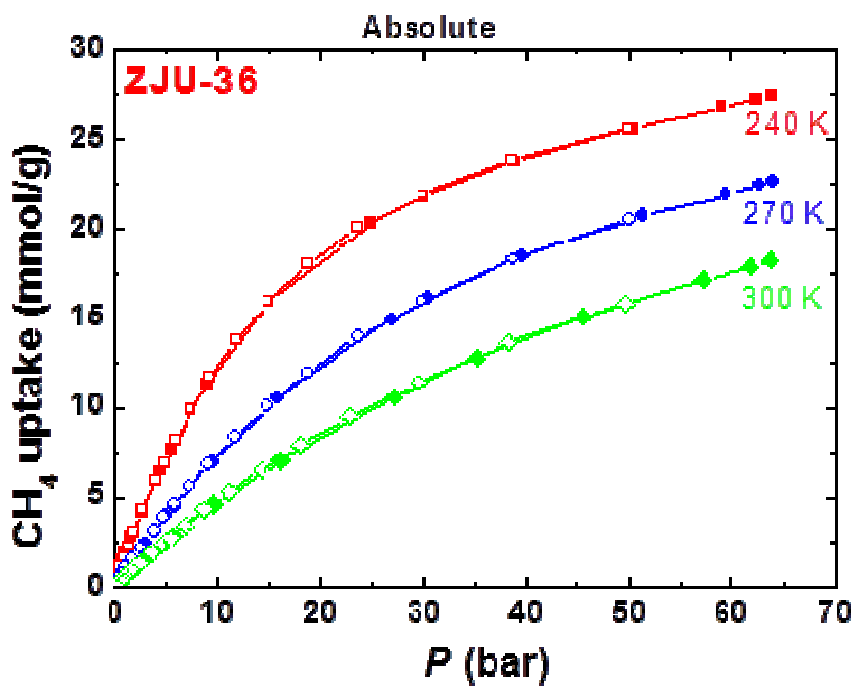


Figure S16. CH₄ (absolute) sorption isotherms of ZJU-36 at different temperatures.

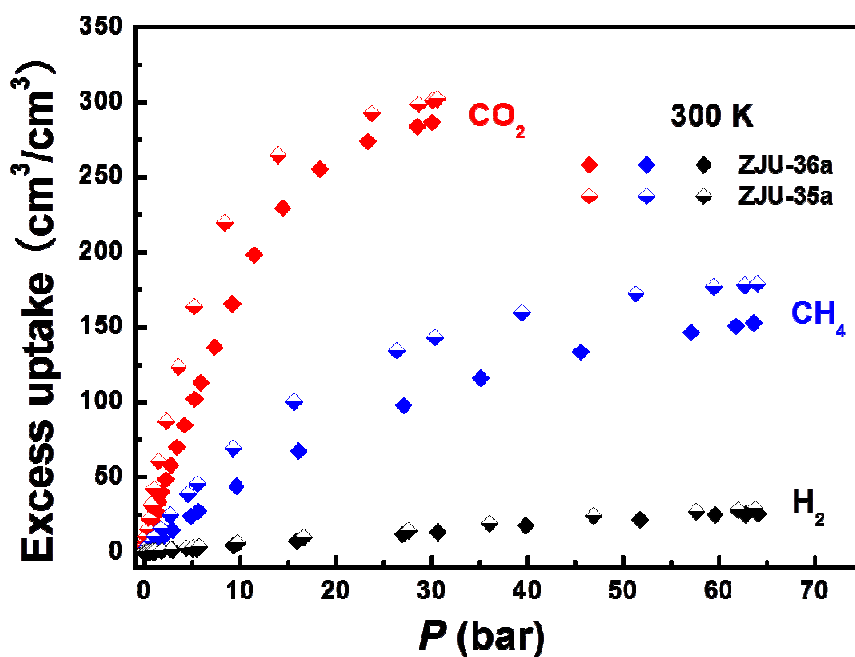


Figure S17. Excess gas sorption isotherms of CO₂ (red), CH₄ (blue) and H₂ (black) of ZJU-35a (solid square) and ZJU-36a (open solid diamond) at 300 K.

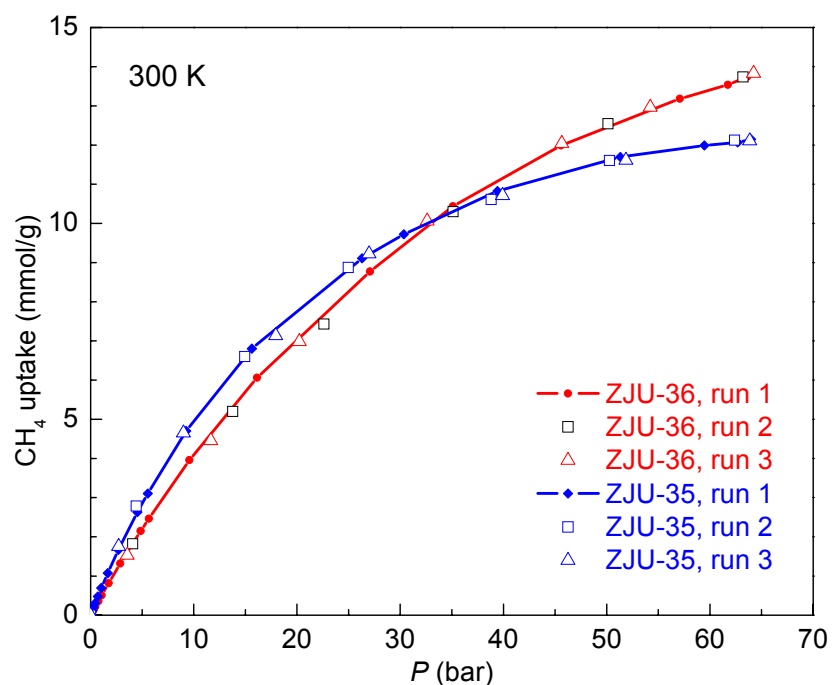


Figure S18. Excess CH₄ adsorption isotherms of ZJU-35 and ZJU-36 at 300 K. The gas uptake amount remains unchanged for the three cycles examined.

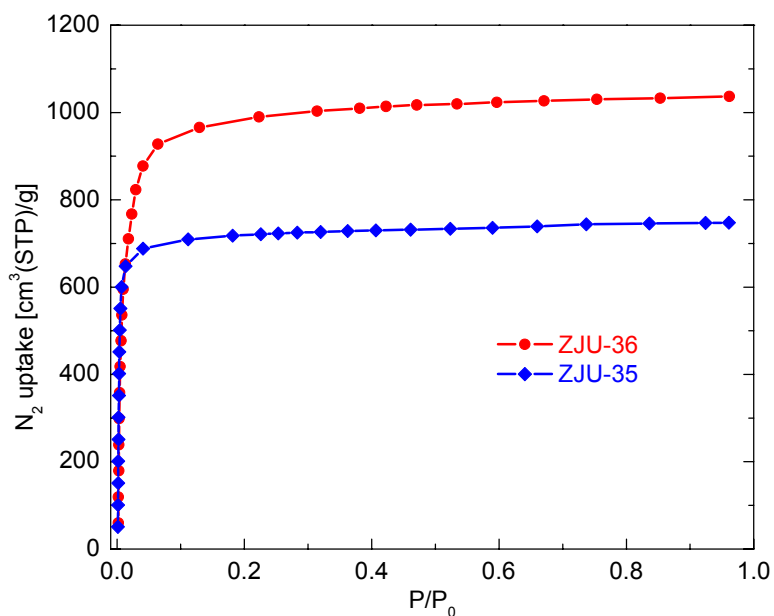


Figure S19. N_2 sorption isotherms of the regenerated **ZJU-35** and **ZJU-36** at 77 K (samples after sorption measurement were exposed to air (50% humidity) for one day, then washed with acetone and reactivated at 100 °C in vacuum).

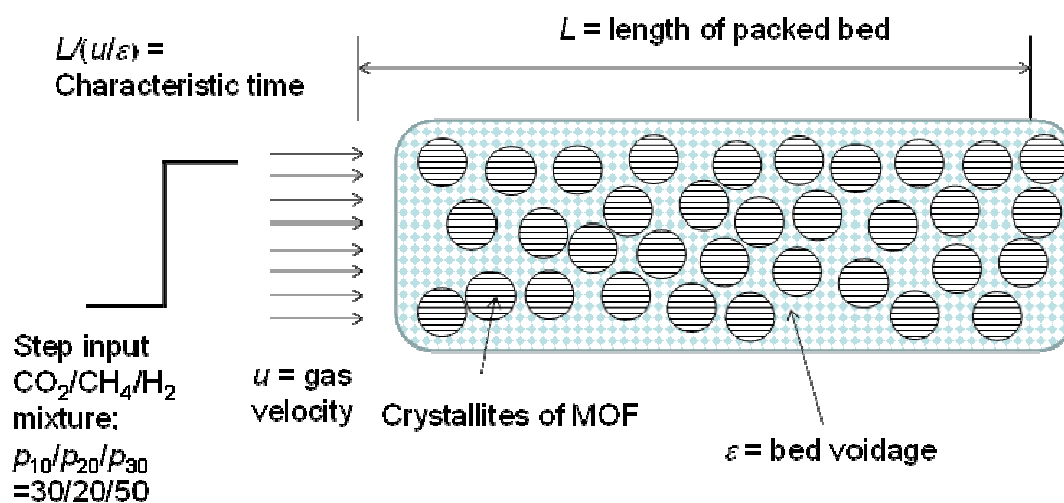


Figure S20. Schematic representation of a packed bed adsorber.

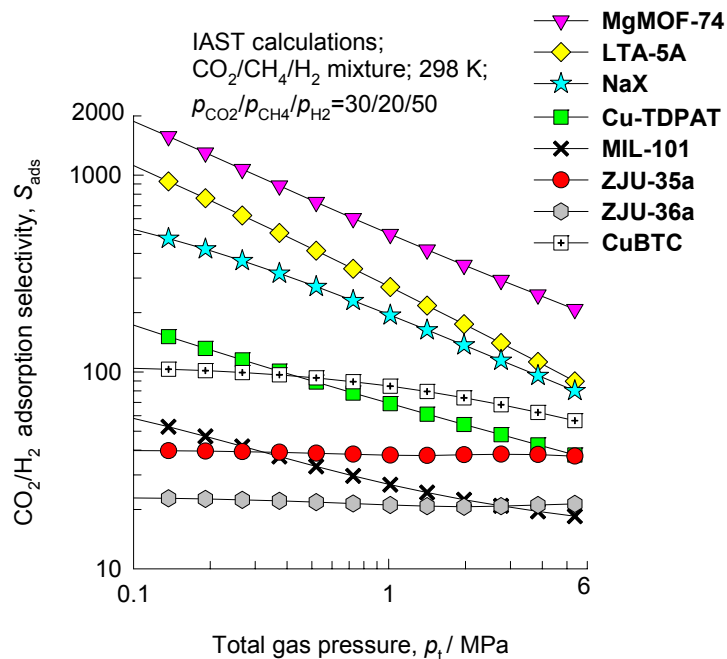


Figure S21. Calculations using Ideal Adsorbed Solution Theory (IAST) of Myers and Prausnitz^{S4} for CO₂/H₂ adsorption selectivities for a ternary CO₂/CH₄/H₂ 30/20/50 gas mixture maintained at isothermal conditions at 298 K.

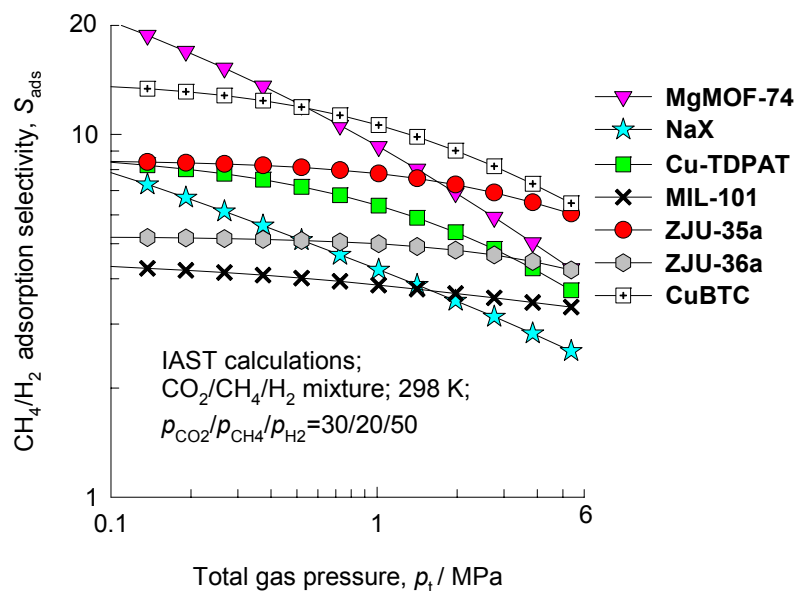


Figure S22. Calculations using Ideal Adsorbed Solution Theory (IAST) of Myers and Prausnitz^{S4} for CH₄/H₂ adsorption selectivities for a ternary CO₂/CH₄/H₂ 30/20/50 gas mixture maintained at isothermal conditions at 298 K.

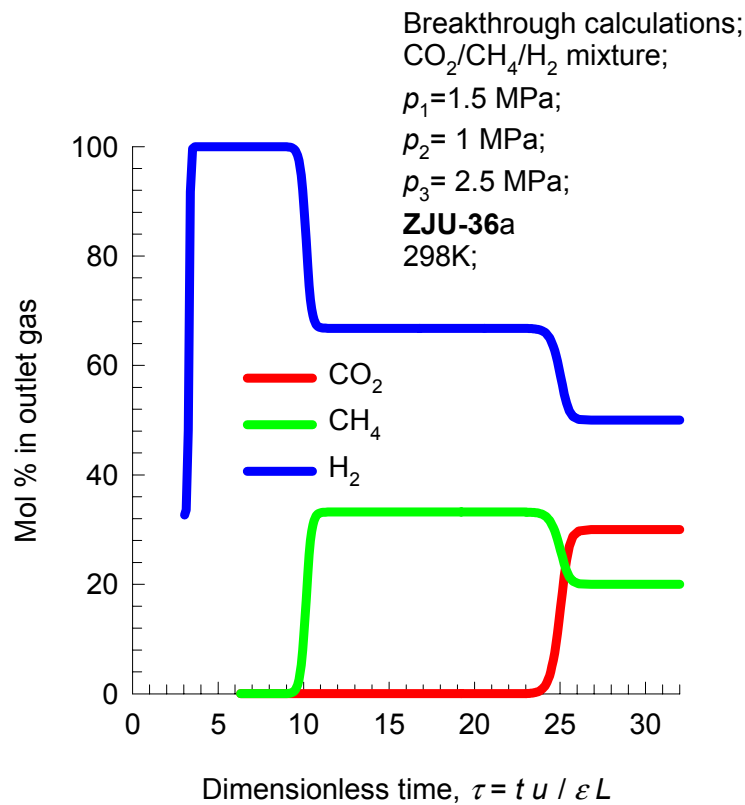


Figure S23. Breakthrough characteristics of an adsorber packed with **ZJU-36a**, maintained at isothermal conditions at 298 K and 5 MPa.

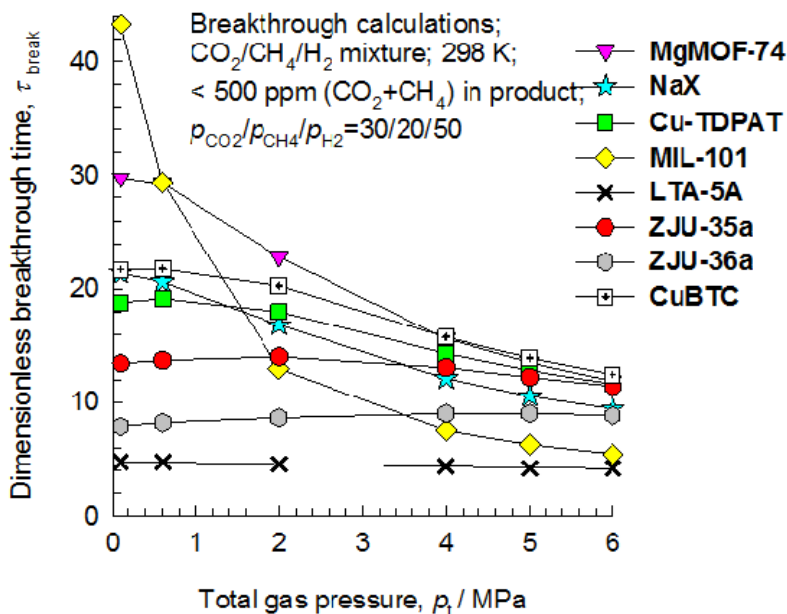


Figure S24. Influence of the total operating pressure on dimensionless breakthrough times.

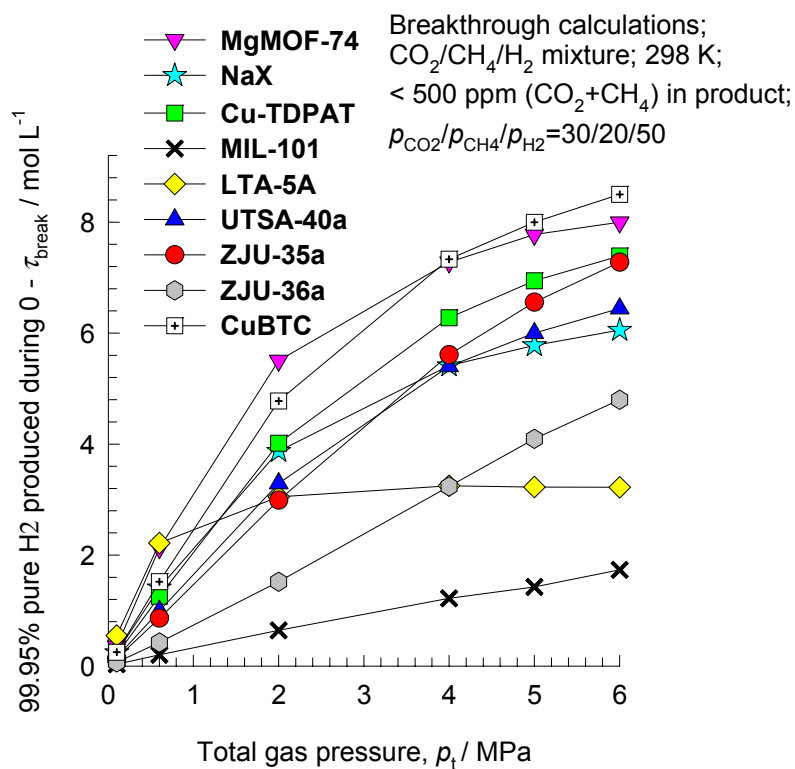


Figure S25. Influence of operating pressure on the number of moles of 99.95%+ pure H_2 produced per L of adsorbent material during the time interval $0 - \tau_{break}$. The breakthrough times, τ_{break} , correspond to those when the outlet gas contains 500 ppm ($CO_2 + CH_4$).

Supporting Tables

Table S1. Crystal data and structure refinements for **ZJU-35** and **ZJU-36**

Compound	ZJU-35	ZJU-36
Formula	C ₂₂ H ₁₆ Cu ₃ O ₁₅	C ₂₆ H ₂₀ Cu ₃ O ₁₅
Formula weight	710.97	763.04
Crystal system, Space group	Cubic, <i>Fm-3m</i>	Cubic, <i>Fm-3m</i>
a (Å)	29.8307(6)	33.6167(7)
Volume (Å ³)	26545.5(9)	37989.6(14)
Z	16	16
ρ (g·cm ⁻³)	0.712	0.534
F(000)	5680	6128
μ (mm ⁻¹)	1.384	0.982
Reflections collected	8749 [R(int) = 0.0294]	7843 [R(int) = 0.0783]
Data / parameters	999 / 61	1367 / 48
Goodness-of-fit on F ²	1.003	1.037
R1 (wR2) [<i>I</i> > 2 σ (<i>I</i>)]	0.0783 (0.2318)	0.0682 (0.1560)
R1 (wR2) (all data)	0.1477 (0.2809)	0.1566 (0.1807)

$$R1 = \sum(|F_o| - |F_c|) / \sum|F_o|, wR2 = [\sum w(F_o^2 - F_c^2)^2 / \sum w(F_o^2)^2]^{0.5}.$$

Table S2. Absolute methane uptakes of some reported MOFs at RT and 60 bar.

MOFs	V_p (cm^3/g)	BET (m^2/g)	D_c (g/cm^3)	Excess uptake (cm^3/g)	Absolute uptake (cm^3/g)	Absolute uptake (cm^3/cm^3)	Deliverable amount (cm^3/cm^3)	Reference
PCN-11	0.91	1931	0.7485	260	315	236	167	S5
NOTT-109	0.850	2110	0.7899	250	299	236	164	S6
NOTT-103	1.157	2958	0.6432	293	362	233	179	S6
NOTT-101	1.080	2805	0.6838	281	341	233	176	S6
NiMOF-74	0.47	1218	1.206	165	193	233	114	S7
NU-125	1.29	3120	0.578	314	398	230	183	S8
NOTT-102	1.268	3342	0.5872	312	388	228	182	S6
MOF-505	0.677	1661	0.9265	202	245	227	136	S6
ZJU-25	1.183	2998	0.6220	290	361	224	177	S9
ZJU-5	1.074	2823	0.6788	268	331	224	165	S10
ZJU-35	1.156	2899	0.6574	269	338	222	177	This work
PCN-61	1.36	3000	0.56	301	381	213	170	S11
MgMOF-74	0.63	1542	0.909	191	229	208	125	S7
PCN-46	1.01	2500	0.619	269	331	205	164	S12
NU-111	2.09	4930	0.409	354	482	197	168	S13
ZJU-36	1.599	4014	0.4958	300	395	196	168	This work
MIL-100	1.10	1900	0.70	213	278	195	164	S14
MIL-101c	2.15	4230	0.44	305	433	191	165	S14
DUT-23(Co)	2.03	4850	0.403	346	468	189	164	S15
UTSA-40a	0.650	1630	0.8270	179	227	188	134	S16
MOF-177	1.89	4500	0.43	314	428	184	166	S17
MOF-5	1.55	3800	0.593	217	310	184	165	S17
PCN-68	2.13	5109	0.38	338	474	180	154	S11
PCN-66	1.63	4000	0.45	308	400	180	149	S11
MOF-205	2.16	4460	0.38	330	460	175	155	S17
DUT-49	2.91	5476	0.3088	364	540	167	146	S18
DUT-25	2.22	4670	0.4157	255	390	162	142	S19
DUT-6	2.02	NA	0.386	277	399	154	138	S20
MOF-210	3.60	6240	0.25	319	536	134	121	S17
MOF-200	3.59	4530	0.22	279	495	109	99	S17

Table S3. CO₂ uptakes of some reported MOFs at RT and 30 bar.

MOFs	V _p (cm ³ /g)	BET (m ² /g)	D _c (g/cm ³)	Excess uptake (cm ³ /g)	Excess uptake (cm ³ /cm ³)	Absolute uptake (cm ³ /g)	Absolute uptake (cm ³ /cm ³)	Reference
NU-111	2.09	4930	0.409	777	318	856	350	S13
PCN-11	0.91	1931	0.7485	416	311	445	333	S21
NiMOF-74	0.47	1218	1.206	260	313	275	332	S7
NOTT-101	1.080	2805	0.6838	445	304	481	328	S22
ZJU-35a	1.156	2899	0.6574	458	301	495	326	This work
NU-125	1.29	3120	0.578	518	299	560	324	S8
PCN-61	1.36	3000	0.56	523	293	568	318	S11
PCN-46	1.01	2500	0.619	476	295	507	314	S12
ZJU-5a	1.074	2823	0.6788	426	289	461	313	S10
MIL-101c	2.15	4230	0.44	641	282	710	313	S14
ZJU-36a	1.599	4014	0.4958	578	287	629	312	This work
MOF-205	2.16	4460	0.38	750	285	821	312	S17
UTSA-20	0.630	1655	0.9096	323	294	343	312	S23
MgMOF-74	0.63	1542	0.909	321	291	342	310	S7
MOF-177	1.89	4500	0.43	654	281	716	308	S17
Cu-TDPAT	0.930	1938	0.7832	360	282	390	306	S24
DUT-25	2.22	4670	0.4157	660	274	732	304	S19
ZJU-25a	1.183	2998	0.6220	447	278	486	302	S9
PCN-16	1.06	2273	0.724	382	276	416	301	S21
IRMOF-6	0.993	2516	0.650	426	277	458	298	S25
DUT-49	2.91	5476	0.3088	851	263	947	292	S18
SNU-77H	1.52	3670	0.586	459	269	490	287	S26
PCN-66	1.63	4000	0.45	573	258	631	284	S11
IRMOF-3	0.853	2160	0.634	415	263	443	281	S25
Cu-BTTri	0.713	1750	0.7891	331	261	353	279	S27
MOF-5	1.55	3800	0.593	422	249	473	279	S11
PCN-68	2.13	5109	0.38	646	245	721	274	S11
IRMOF-11	0.830	2096	0.760	325	247	352	268	S25
MIL-100	1.10	1900	0.70	339	237	375	262	S14
SNU-50'	1.08	2300	0.650	361	235	397	258	S28
Be-BTB ^b	1.701	4030	0.4232	547	231	599	253	S27
NU-100	2.82	6143	0.2791	793	221	896	250	S29.
PCN-80	1.47	3850	0.574	376	216	424	243	S30
UTSA-40	0.650	1630	0.8270	259	214	285	236	S16
HKUST-1	0.701	1781	0.879	240	211	263	231	S25
MOF-505	0.603	1547	0.9265	226	209	246	228	S25
MOF-210	3.60	6240	0.25	766	192	884	221	S17
ZIF-8	0.650	1980	0.924	194	179	215	199	S21
MOF-200	3.59	4530	0.22	766	169	883	194	S17

Table S4. Structural data on the different adsorbents evaluated in this study for comparison purposes. The data for MgMOF-74 and NaX are from Herm et al.^{S27} and Krishna and Long^{S31}. The data for MIL-101 are taken from Chowdhury et al.^{S32} The data for Cu-TDPAT are from Wu et al.^{S33} The data for LTA-5A are from Pakseresht et al.^{S34} and Sircar and Golden.^{S35}

MOFs	Surface area $\text{m}^2 \text{g}^{-1}$	Pore volume $\text{cm}^3 \text{g}^{-1}$	Framework density kg m^{-3}
MgMOF-74	1800	0.573	905
MIL-101	2674	1.38	440
CuBTC	2097	0.848	879
Cu-TDPAT	1938	0.93	782
NaX zeolite	950	0.280	1421
LTA-5A	450	0.250	1508
ZJU-35a	2958	1.156	657
ZJU-36a	3243	1.599	496

Table S5. Dual-site Langmuir-Freundlich parameters for adsorption of CO_2 , and CH_4 in ZJU-35a. The fits for CO_2 are based on high pressure isotherm data measured at 240 K, 270 K, and 300 K.

	Site A				Site B			
	$q_{A,\text{sat}}$ mol kg^{-1}	b_{A0} $\text{Pa}^{-\nu_i}$	E_A kJ mol^{-1}	ν_A dimensionless	$q_{B,\text{sat}}$ mol kg^{-1}	b_{B0} $\text{Pa}^{-\nu_i}$	E_B kJ mol^{-1}	ν_B dimensionless
CO_2	8.6	1.10×10^{-13}	27.6	1	7.4	4.12×10^{-10}	23.6	1
CH_4	14	1.13×10^{-9}	15	1				

Table S6. 1-site Langmuir parameters for pure H_2 isotherms in ZJU-35a. The fits are for a temperature of 298 K.

	$q_{A,\text{sat}}$ mol kg^{-1}	b_A $\text{Pa}^{-\nu_i}$	ν_A dimensionless
H_2	19	3.4×10^{-8}	1

Table S7. Dual-site Langmuir-Freundlich parameters for adsorption of CO₂, and CH₄ in ZJU-36a. The fits for CO₂ are based on high pressure isotherm data measured at 240 K, 270 K, and 300 K.

	Site A				Site B			
	$q_{A,sat}$ mol kg ⁻¹	b_{A0} Pa ^{-ν_i}	E_A kJ mol ⁻¹	ν_A dimensionless	$q_{B,sat}$ mol kg ⁻¹	b_{B0} Pa ^{-ν_i}	E_B kJ mol ⁻¹	ν_B dimensionless
CO ₂	8.6	1.10×10 ⁻¹³	27.6	1	7.4	4.12×10 ⁻¹⁰	23.6	1
CH ₄	14	1.13×10 ⁻⁹	15	1				

Table S8. 1-site Langmuir parameters for pure H₂ isotherms in ZJU-36a. The fits are for a temperature of 298 K.

	$q_{A,sat}$ mol kg ⁻¹	b_A Pa ^{-ν_i}	ν_A dimensionless
H ₂	19	3.4×10 ⁻⁸	1

Table S9. Dual-Langmuir-Freundlich parameter fits for MgMOF-74 (= Mg₂(dobdc) = CPO-27-Mg). These CO₂ parameters were determined by fitting adsorption isotherms for temperatures ranging from 278 K to 473 K; the fit parameters are those reported earlier in the work of Mason et al.^{S36} The CH₄ parameters were determined by fitting adsorption isotherm data reported in the works of and He et al.^{S37}, Dietzel et al.^{S7} and Bao et al.^{S38} The H₂ parameters are obtained from absolute uptake data in MgMOF-74 at 298 K reported by Yaghi,^{S39} a document that is available on the web. The uptake data is at 298 K, and therefore the fit parameters are valid only for 298 K.

	Site A				Site B			
	$q_{A,sat}$ mol kg ⁻¹	b_{A0} Pa ^{-ν_i}	E_A kJ mol ⁻¹	ν_A dimensionless	$q_{B,sat}$ mol kg ⁻¹	b_{B0} Pa ^{-ν_i}	E_B kJ mol ⁻¹	ν_B dimensionless
CO ₂	6.8	2.44×10 ⁻¹¹	42	1	9.9	1.39×10 ⁻¹⁰	24	1
CH ₄	11	7.48×10 ⁻¹⁰	18.2	1	5	1.64×10 ⁻¹¹	18.2	1
H ₂	36	2.1×10 ⁻⁸		1				

Table S10. Dual-site Langmuir parameters for pure CO₂, CH₄, and H₂ isotherms in CuBTC.

	Site A				Site B			
	$q_{A,sat}$ mol kg ⁻¹	b_{A0} Pa ^{-v_i}	E_A kJ mol ⁻¹	v_A dimensionless	$q_{B,sat}$ mol kg ⁻¹	b_{B0} Pa ^{-v_i}	E_B kJ mol ⁻¹	v_B dimensionless
CO ₂	16.3	1.42×10 ⁻¹⁰	25.7	1	2.1	8.92×10 ⁻²⁰	72	1
CH ₄	15.6	1.11×10 ⁻⁹	15.7	1				
H ₂	32	1.34×10 ⁻⁹	6.9	1				

Table S11. Dual-Langmuir-Freundlich parameter fits for Cu-TDPAT. The parameters are those reported in the work of Wu et al.^{S33} Note that for CH₄ and H₂, the data is available only at 298 K, and so information on the heat of adsorption is provided. There was an unfortunate typographical error in the CO parameters reported in Table 3 of Supporting Information accompanying the paper by Wu et al;^{S33} we have therefore also included the correct parameters for CO (not considered in this work) in the Table below. The breakthrough and IAST calculations reported by Wu et al.^{S33} were performed with the correct parameter sets.

	Site A				Site B			
	$q_{A,sat}$ mol kg ⁻¹	b_{A0} Pa ^{-v_i}	E_A kJ mol ⁻¹	v_A dimensionless	$q_{B,sat}$ mol kg ⁻¹	b_{B0} Pa ^{-v_i}	E_B kJ mol ⁻¹	v_B dimensionless
CO ₂	0.46	1.33×10 ⁻¹⁶	72	1.2	23.9	2.91×10 ⁻⁹	23.8	0.75
CO	23	2.47×10 ⁻⁸	13.2	0.8	2	6.75×10 ⁻¹⁵	17.7	1.8
CH ₄	16	5.77×10 ⁻⁷		1				
H ₂	38.5	2.6×10 ⁻⁸		1				

Table S12. Dual-site Langmuir parameters for pure component isotherms in MIL-101. The fits for CO₂, and CH₄ and H₂ are based on the experimental data of Chowdhury et al.^{S32} The fits for pure H₂ isotherms in MIL-101 are based on the experimental data of Latroche et al.^{S40}, available only at 298 K. There was an unfortunate typographical error in the H₂ parameters reported in Table 12 of Supporting Information accompanying the paper by Wu et al.^{S33} The breakthrough and IAST calculations reported by Wu et al.^{S33} were performed with the correct parameter sets as given below.

	Site A				Site B			
	$q_{A,sat}$ mol kg ⁻¹	b_{A0} Pa ^{-ν_i}	E_A kJ mol ⁻¹	ν_A dimensionless	$q_{B,sat}$ mol kg ⁻¹	b_{B0} Pa ^{-ν_i}	E_B kJ mol ⁻¹	ν_B dimensionless
CO ₂	47	2.22×10 ⁻¹⁰	17.5	1	1.1	2.95×10 ⁻¹¹	36	1
CH ₄	34	1.79×10 ⁻⁹	9.9	1				
H ₂	60	1.41×10 ⁻⁸		1				

Table S13. Dual-site Langmuir parameter for adsorption of CO₂, CH₄ and H₂ in NaX zeolite. These parameters were determined by fitting adsorption isotherm data reported in the works of Belmabkhout et al.^{S41} and Cavenati et al.^{S42}, after converting the excess data to absolute loadings.

	Site A				Site B			
	$q_{A,sat}$ mol kg ⁻¹	b_{A0} Pa ^{-ν_i}	E_A kJ mol ⁻¹	ν_A dimensionless	$q_{B,sat}$ mol kg ⁻¹	b_{B0} Pa ^{-ν_i}	E_B kJ mol ⁻¹	ν_B dimensionless
CO ₂	3.5	3.64×10 ⁻¹³	35	1	5.2	6.04×10 ⁻¹¹	35	1
CH ₄	4	3.66×10 ⁻¹⁰	14	1	5	3.75×10 ⁻⁹	14	1
H ₂	18	2.43×10 ⁻⁹	6	1				

Table S14. 2-site Langmuir-Freundlich parameters for pure CO₂, CH₄ and H₂ isotherms in LTA-5A zeolite. The fits for pure CO₂, CH₄ are derived from re-fitting the experimental data at 303 K presented in Table 1 of Pakseresht *et al.*^{S34} The isotherm fit for H₂ is based on the data presented in Figure 6 of Sircar and Golden,^{S35} that was combined with Configurational-Bias Monte Carlo simulation data.

	$q_{A,sat}$ mol kg ⁻¹	b_A Pa ^{-v_A}	v_A dimensionless	$q_{B,sat}$ mol kg ⁻¹	b_B Pa ^{-v_B}	v_B dimensionless
CO ₂	1.84	1.89×10 ⁻⁴	1.24	2.1	8.51×10 ⁻⁴	0.64
CH ₄	2	5.77×10 ⁻⁶	1			
H ₂	15	2.05×10 ⁻⁸	1			

Adsorbents compared: The performance of six different adsorbents were compared for separation of CO₂/CH₄/H₂ mixtures. The structural data are provided in Table S2.

Fitting of pure component isotherms

ZJU-35a and ZJU-36a: The pure component isotherm data for CO₂, for three different temperatures 240 K, 270 K, and 300 K were fitted with the dual-site Langmuir-Freundlich model

$$q = q_{A,sat} \frac{b_A p^{v_A}}{1 + b_A p^{v_A}} + q_{B,sat} \frac{b_B p^{v_B}}{1 + b_B p^{v_B}} \quad (1)$$

with T -dependent parameters b_A , and b_B

$$b_A = b_{A0} \exp\left(\frac{E_A}{RT}\right); \quad b_B = b_{B0} \exp\left(\frac{E_B}{RT}\right) \quad (2)$$

The isotherm parameters are provided in Tables S5 and S7.

The pure component isotherms of CH₄, and H₂ in do not demonstrate any inflection characteristics and the single-site Langmuir model

$$q = \frac{q_{sat} b p}{1 + b p} \quad (3)$$

provides an adequately good representation of the absolute component loadings. The

isotherm parameters are provided in Tables S6 and S8.

MgMOF-74: For evaluating the performance of MgMOF-74 the pure component isotherm data for CO₂ and CH₄, were obtained from the works of Mason et al.,^{S36} Herm et al.,^{S27,S43} He et al. and Dietzel et al.^{S44-S48} The measured experimental data on excess loadings were converted to absolute loadings for fitting purposes. The temperature-dependent fit parameters are specified in Table S8. The pure component H₂ uptake data at 298 K are reported by Yaghi^{S39} in a document that is available on the web. The fit parameters are provided in Table S9.

CuBTC: The measured experimental data on excess loadings published by Chowdhury et al.^{S32} on pure component isotherms for CO₂, and CH₄ at 295 K, 318 K, and 353 K in CuBTC were first converted to absolute loadings using the Peng-Robinson equation of state for estimation of the fluid phase molar densities within the pores. These data sets were combined with the high pressure experimental isotherm data of Moellmer et al.^{S49} for absolute loadings for CO₂, and CH₄ and H₂ in CuBTC at various temperatures. The combined data sets were fitted to obtain the parameters reported in Table S10.

Cu-TDPAT: For evaluating the performance of Cu-TDPAT the pure component isotherm data were obtained from the works of Wu et al.^{S33} The parameter sets are provided in Table S11.

MIL-101: For evaluating the performance of MIL, the pure component isotherm data for CO₂, and CH₄ were obtained from the work of Chowdhury et al.^{S32} The temperature-dependent fit parameters are specified in Table S11. The pure component isotherm data for pure component H₂ at 298 K are reported by Latroche et al.^{S40}; these data were fitted with the Langmuir constants specified in Table S12.

NaX zeolite: For evaluating the performance of NaX zeolite we used the pure component isotherm data for CO₂, CH₄, and H₂ reported by Belmabkhout et al.^{S41} and

Cavenati et al.^{S42} for a variety of temperatures. The excess loading reported in these papers are converted to absolute loadings using a pore volume of 0.28 cm³/g, along with the Peng-Robinson equation of state for estimation of the fluid phase densities within the pores. The temperature-dependent fit parameters are specified in Table S13.

LTA-5A zeolite: Table S13 presents the 2-site Langmuir-Freundlich parameters for pure CO₂, CH₄ and H₂ isotherms in LTA-5A zeolite. These fits are derived from fitting the data presented in Table 1 of Pakseresht et al.^{S34}, along with Figure 6 of Sircar and Golden.^{S35}

Isosteric heat of adsorption: The isosteric heat of adsorption, Q_{st} , defined as

$$Q_{st} = RT^2 \left(\frac{\partial \ln p}{\partial T} \right)_q \quad (4)$$

were determined using the pure component isotherm fits. The calculations of $-Q_{st}$ are based on the use of the Clausius-Clapeyron equation, using *numerical* procedures for differentiation of the dual-Langmuir-Freundlich model.

Calculations of adsorption selectivity: The selectivity of preferential adsorption of component 1 over component 2 in a mixture containing 1 and 2, perhaps in the presence of other components too, can be formally defined as

$$S_{ads} = \frac{q_1/q_2}{p_1/p_2} \quad (5)$$

In equation (5), q_1 and q_2 are the *absolute* component loadings of the adsorbed phase in the mixture. In all the calculations to be presented below, the calculations of S_{ads} are based on the use of the Ideal Adsorbed Solution Theory (IAST) of Myers and Prausnitz.^{S4} These calculations are carried out using the pure component isotherm fits of absolute component loadings.

Packed bed adsorber breakthrough simulation methodology: In order to obtain a realistic appraisal of the separation characteristics of various MOFs for H₂ purification

we perform transient breakthrough calculations. The methodology followed is identical to the ones described in detail in earlier works.^{S31, S33, S37, S43-S46, S50} Experimental validation of the breakthrough simulation methodology is also available in the published literature.^{S33, S37, S51}

The following parameter values were used in the simulations to be reported below: $L = 0.1$ m; $\varepsilon = 0.4$; $v = 0.1$ m/s (at inlet). When comparing different materials, the fractional voidage is held constant at $\varepsilon = 0.4$. This implies the volumes of adsorbents used in the fixed bed are the same for ZJU-35a, ZJU-36a, CuBTC, MgMOF-74, Cu-TDPAT, MIL-101, NaX, and LTA-5A. The total mass of the adsorbents used is governed by the framework density.

Ternary 30/20/50 CO₂/CH₄/H₂ breakthrough simulations: For industrial production of H₂, impurities such as CO₂, and CH₄ need to be reduced to extremely low levels, typically lower than 500 ppm. Figures 4c and S23 show typical concentration profiles at the exit of the adsorber packed with ZJU-35a, and ZJU-36a, respectively, and maintained at isothermal conditions at 298 K, and operating at a total pressure of 5 MPa. During the initial period of the fixed bed operation it is possible to recover hydrogen gas of the required purity. From the exit gas concentrations we can determine the ppm (CO₂ + CH₄) in outlet gas as a function of the dimensionless time, τ , defined by dividing the actual time, t , by the characteristic time, $\frac{L}{v}$. When the composition in the exit gas reaches a certain desired purity level, the adsorption cycle needs to be terminated and the contents of the bed regenerated. Longer breakthrough times are desirable because this reduces the frequency of regeneration. We choose the purity level to be 500 ppm (CO₂ + CH₄) in outlet gas that is typical of industrial requirements. When this purity level is reached, the corresponding dimensionless breakthrough time, τ_{break} , can be determined.

Notation

b_A dual-Langmuir-Freundlich constant for species i at adsorption site A, Pa^{- v_i}

b_B	dual-Langmuir-Freundlich constant for species i at adsorption site B, $\text{Pa}^{-\nu_i}$
L	length of packed bed adsorber, m
p_i	partial pressure of species i in mixture, Pa
p_t	total system pressure, Pa
q_i	component molar loading of species i , mol kg^{-1}
q_t	total molar loading in mixture, mol kg^{-1}
$q_{\text{sat,A}}$	saturation loading of site A, mol kg^{-1}
$q_{\text{sat,B}}$	saturation loading of site B, mol kg^{-1}
Q_{st}	isosteric heat of adsorption, J mol^{-1}
R	gas constant, $8.314 \text{ J mol}^{-1} \text{ K}^{-1}$
S_{ads}	adsorption selectivity, dimensionless
t	time, s
T	absolute temperature, K
u	superficial gas velocity in packed bed, m s^{-1}
v	interstitial gas velocity in packed bed, m s^{-1}
z	distance along the adsorber, m

Greek letters

ε	voidage of packed bed, dimensionless
ν	exponent in dual-Langmuir-Freundlich isotherm, dimensionless
ρ	framework density, kg m^{-3}
τ	time, dimensionless
τ_{break}	breakthrough time, dimensionless

Subscripts

i	referring to component i
A	referring to site A
B	referring to site B

References:

- S1. Oxford Diffraction Ltd. CrysAlisPro, Version 1.171.33.56, **2010**.
- S2. G. M. Sheldrick, Program for Structure Refinement, University of Göttingen, Germany, **1997**.
- S3. A. L. Spek, *J. Appl. Crystallogr.* **2003**, *36*, 7.
- S4. A. L. Myers, J. M. Prausnitz, *A.I.Ch.E.J.* **1965**, *11*, 121.
- S5. X.-S. Wang, S. Ma, K. Rauch, J. M. Simmons, D. Yuan, X. Wang, T. Yildirim, W. C. Cole, J. J. López, A. d. Meijere, H.-C. Zhou, *Chem. Mater.* **2008**, *20*, 3145.
- S6. Y. He, W. Zhou, T. Yildirim, B. Chen, *Energy Environ. Sci.* **2013**, *6*, revision submitted.
- S7. P. D. C. Dietzel, V. Besikiotis, R. Blom, *J. Mater. Chem.* **2009**, *19*, 7362.
- S8. C. E. Wilmer, O. K. Farha, T. Yildirim, I. Eryazici, V. Krungleviciute, A. A. Sarjeant, R. Q. Snurr, J. T. Hupp, *Energy Environ. Sci.* **2013**, *6*, 1158.
- S9. X. Duan, J. Yu, J. Cai, Y. He, C. Wu, W. Zhou, T. Yildirim, Z. Zhang, S. Xiang, M. O'Keeffe, B.

- Chen, G. Qian, *Chem. Commun.* **2013**, *49*, 2043.
- S10. X. Rao, J. Cai, J. Yu, Y. He, C. Wu, W. Zhou, T. Yildirim, B. Chen, G. Qian, *Chem. Commun.* **2013**, *49*, revision submitted.
- S11. D. Yuan, D. Zhao, D. Sun, H.-C. Zhou, *Angew. Chem. Int. Ed.* **2010**, *49*, 5357.
- S12. D. Zhao, D. Yuan, A. Yakovenko, H.-C. Zhou, *Chem. Commun.* **2010**, *46*, 4196.
- S13. Y. Peng, G. Srinivas, C. E. Wilmer, R. Q. Snurr, J. T. Hupp, T. Yildirim, O. K. Farha, *Chem. Commun.* **2013**, *49*, 2992.
- S14. P. L. Llewellyn, S. Bourrelly, C. Serre, A. Vimont, M. Daturi, L. Hamon, G. D. Weireld, J.-S. Chang, D.-Y. Hong, Y. K. Hwang, S. H. Jhung, G. Férey, *Langmuir* **2008**, *24*, 7245.
- S15. N. Klein, I. Senkovska, I. A. Baburin, R. Grünker, U. Stoeck, M. Schlichtenmayer, B. Streppel, U. Mueller, S. Leoni, M. Hirscher, S. Kaskel, *Chem. Eur. J.* **2011**, *17*, 13007.
- S16. Y. He, S. Xiang, Z. Zhang, S. Xiong, C. Wu, W. Zhou, T. Yildirim, R. Krishna, B. Chen, *J. Mater. Chem. A* **2013**, *23*, 2543.
- S17. H. Furukawa, N. Ko, Y. B. Go, N. Aratani, S. B. Choi, E. Choi, A. Ö. Yazaydin, R. Q. Snurr, M. O'Keeffe, J. Kim, O. M. Yaghi, *Science* **2010**, *329*, 424.
- S18. U. Stoeck, S. Krause, V. Bon, I. Senkovska, S. Kaskel, *Chem. Commun.* **2012**, *48*, 10841.
- S19. R. Grünker, V. Bon, A. Heerwig, N. Klein, P. Müller, U. Stoeck, I. A. Baburin, U. Mueller, I. Senkovska, S. Kaskel, *Chem. Eur. J.* **2012**, *18*, 13299.
- S20. N. Klein, I. Senkovska, K. Gedrich, U. Stoeck, A. Henschel, U. Mueller, S. Kaskel, *Angew. Chem. Int. Ed.* **2009**, *48*, 9954.
- S21. J. M. Simmons, H. Wu, W. Zhou, T. Yildirim, *Energy Environ. Sci.* **2011**, *4*, 2177.
- S22. X. Lin, I. Telepeni, A. J. Blake, A. Dailly, C. M. Brown, J. M. Simmons, M. Zoppi, G. S. Walker, K. M. Thomas, T. J. Mays, P. Hubberstey, N. R. Champness, M. Schröder, *J. Am. Chem. Soc.* **2009**, *131*, 2159.
- S23. Z. Guo, H. Wu, G. Srinivas, Y. Zhou, S. Xiang, Z. Chen, Y. Yang, W. Zhou, M. O'Keeffe, B. Chen, *Angew. Chem. Int. Ed.* **2011**, *50*, 3178.
- S24. B. Li, Z. Zhang, Y. Li, K. Yao, Y. Zhu, Z. Deng, F. Yang, X. Zhou, G. Li, H. Wu, N. Nijem, Y. J. Chabal, Z. Lai, Y. Han, Z. Shi, S. Feng, J. Li, *Angew. Chem. Int. Ed.* **2011**, *51*, 1412.
- S25. A. R. Millward, O. M. Yaghi, *J. Am. Chem. Soc.* **2005**, *127*, 17998.
- S26. H. J. Park, D.-W. Lim, W. S. Yang, T.-R. Oh, M. P. Suh, *Chem. Eur. J.* **2011**, *17*, 7251.
- S27. Z. R. Herm, J. A. Swisher, B. Smit, R. Krishna, J. R. Long, *J. Am. Chem. Soc.* **2011**, *133*, 5664.
- S28. T. K. Prasad, D. H. Hong, M. P. Suh, *Chem. Eur. J.* **2010**, *16*, 14043.
- S29. O. K. Farha, A. O. Yazaydin, I. Eryazici, C. D. Malliakas, B. G. Hauser, M. G. Kanatzidis, S. T. Nguyen, R. Q. Snurr, J. T. Hupp, *Nat. Chem.* **2010**, *2*, 944.
- S30. W. Lu, D. Yuan, T. A. Makal, J.-R. Li, H.-C. Zhou, *Angew. Chem. Int. Ed.* **2012**, *51*, 1508.
- S31. R. Krishna, J. R. Long, *J. Phys. Chem. C* **2011**, *115*, 12941.
- S32. P. Chowdhury, S. Mekala, F. Dreisbach, S. Gumma, *Micropor. Mesopor. Mater.* **2012**, *152*, 246.
- S33. H. Wu, K. Yao, Y. Zhu, B. Li, Z. Shi, R. Krishna, J. Li, *J. Phys. Chem. C* **2012**, *116*, 16609.
- S34. S. Pakseresht, M. Kazemeini, M. M. Akbarnejad, *Sep. Purif. Technol.* **2002**, *28*, 53.
- S35. S. Sircar, T. C. Golden, *Sep. Sci. Technol.* **2000**, *35*, 667.
- S36. J. A. Mason, K. Sumida, Z. R. Herm, R. Krishna, J. R. Long, *Energy Environ. Sci.* **2011**, *3*, 3030.
- S37. Y. He, R. Krishna, B. Chen, *Energy Environ. Sci.* **2012**, *5*, 9107.

- S38. Z. Bao, L. Yu, Q. Ren, X. Lu, S. Deng, *J. Colloid Interface Sci.* **2011**, *353*, 549.
- S39. O. M. Yaghi, Hydrogen Storage in Metal Organic Frameworks, www.hydrogen.energy.gov/pdfs/review11/st049_yaghi_2011_p.pdf, University of California Los Angeles, California, **2011**.
- S40. M. Latroche, S. Surblé, C. Serre, C. Mellot-Draznieks, P. L. Llewellyn, J. H. Lee, J. S. Chang, S. H. Jung, G. Férey, *Angew. Chem. Int. Ed.* **2006**, *45*, 8227.
- S41. Y. Belmabkhout, G. Pirngruber, E. Jolimaître, A. Methivier, *Adsorption* **2007**, *13*, 341.
- S42. S. Cavenati, C. A. Grande, A. E. Rodrigues, *J. Chem. Eng. Data* **2004**, *49*, 1095.
- S43. Z. R. Herm, R. Krishna, J. R. Long, *Micropor. Mesopor. Mater.* **2012**, *151*, 481.
- S44. Y. He, Z. Zhang, S. Xiang, F. R. Fronczek, R. Krishna, Chen, B. *Chem. Eur. J.* **2012**, *18*, 613.
- S45. Y. He, Z. Zhang, S. Xiang, F. R. Fronczek, R. Krishna, B. Chen, *Chem. Commun.* **2012**, *48*, 6493.
- S46. Y. He, Z. Zhang, S. Xiang, H. Wu, F. R. Fronczek, W. Zhou, R. Krishna, M. O'Keeffe, B. Chen, *Chem. Eur. J.* **2012**, *18*, 1901.
- S47. Y. He, W. Zhou, R. Krishna, B. Chen, *Chem. Commun.* **2012**, *48*, 11813.
- S48. P. D. C. Dietzel, V. Besikiotis, R. Blom, *J. Mater. Chem.* **2009**, *19*, 7362.
- S49. J. Moellmer, A. Moeller, F. Dreisbach, R. Glaeser, R. Staudt, *Micropor. Mesopor. Mater.* **2011**, *138*, 140.
- S50. R. Krishna, *Micropor. Mesopor. Mater.* **2012**, *156*, 217.
- S51. E. D. Bloch, W. L. Queen, R. Krishna, J. M. Zadrozny, C. M. Brown, J. R. Long, *Science* **2012**, *335*, 1606.